Temperature, Airflow and Moisture Patterns in Attic Roofs

Submitted to:

BC HOUSING

July 2020

BCIT Building Science Centre of Excellence

British Columbia Institute of Technology
3700 Willingdon Avenue,
Burnaby, British Columbia,
V5G 3H2

Acknowledgments

The authors are grateful for the financial and in-kind support provided by BC Housing, the Canada Research Chair (CRC), and the School of Construction and the Environment at the British Columbia Institute of Technology (BCIT).

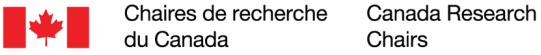

Executive Summary

Energy efficiency and hygrothermal performance are a few of the main considerations during the design and construction of an attic roof system. In the past eight to nine decades, several studies have been conducted on building durable and energy-efficient attic roofs. Most of these findings recommend ventilating an attic space to avoid mould growth and reduce the heating/cooling load of the system, while others cite ventilation as a potential source of the problems. To propose a design solution to such problem, it is essential to develop an advanced understanding of attic ventilation. Through the use of computational fluid dynamics (CFD), this research aims to provide a more in-depth insight into the heat, air, and moisture transfers in an attic roof.

This study examines the airflow distributions, attic air and roof sheathing temperatures, attic ventilation rates, and heating and cooling loads of an attic roof in four attic ventilation scenarios (sealed attic, buoyancy-driven attic ventilation, and two buoyancy- and wind-driven attic ventilation cases) under winter and summer weather conditions. Moreover, the hygrothermal response of the attic roof sheathing for cases with different attic insulation levels and ceiling airtightness are investigated.

The research results show that attic ventilation in both cold and coastal climates is significantly affected by wind pressure and solar radiation. In the absence of wind and solar radiation, buoyancy-induced ventilation in the winter is more than two times that in the summer (~4 ACH [air exchange per hour] vs 1.5 ACH). In the absence of wind, attic ventilation increases as solar radiation increases. The increments due to solar radiation can be as high as 4 ACH during the summer and 2 ACH during the winter. For wind pressure of 0.6 Pa and 2 Pa (wind speed of 1 m/s and 1.8 m/s), the attic ventilation rates in the winter increase by 2.5 and 5.0 times compared to no wind pressure (only stack effect ~4 ACH). Unlike buoyancy-induced ventilation, wind-induced ventilation is less sensitive to solar radiation and delivers similar ACH in both winter and summer. In general, baffle size (size of an air gap between the roof sheathing and insulation) has an impact on attic ventilation rate and airflow distribution, but has a lesser effect on attic air temperature. The effect of baffle size is not significant when the ventilation is driven by a stack-effect. However, for wind pressure of 2 Pa, the ACH in the attics with a 2" and 3" baffle size is 38.5% and 52.5% higher, respectively, than the ACH in an attic with a 1" baffle size. From an energy perspective, the CFD simulation results show that attic ventilation in winter poses an energy penalty, whereas

it is a benefit during the summer period because it removes the hot air from the attic space and reduces cooling load and energy demand.

The simulation results also show that in addition to the attic ventilation rate, wind pressure and solar radiation shape the airflow pattern in an attic space. At a relatively high wind pressure (2 Pa in this report) and absence of solar radiation, the incoming air enters through the soffit vent, flows underneath the roof sheathing, and exits at the ridge vent without mixing with the attic air (without diluting the attic air). At a lower wind pressure and in buoyancy-driven cases, the air flows predominately over the insulation as opposed to under the roof sheathing. The coupled CFD and HAM modeling study results show that the roof sheathing maintains smaller amounts of moisture under a reduced insulation thickness. Furthermore, the roof sheathing areas that are in close proximity to the attic baffle near the soffit region are most susceptible to moisture damage. The effect of ceiling leakage is found to be greater in the upper parts of the sheathing when compared to the middle and lower sections for air leakage at the ceiling center point.

Table of Contents

List of Figures

List of Tables

1. Introduction

It is a common practice to design and build sloped roofs with openings at soffits and ridges to promote airflow through an attic roof system. In cold and mild climates, the airflow is intended to control moisture in the attic space, whereas in a warm climate, it is meant to cool the roof and increase its thermal performance. Ventilating attics can also minimize the ice dams formed near eaves and prolong roof shingles' service life. Ventilating for one of these drivers can have a contrary effect on the other objectives. For example, ventilating the attic to remove moisture during winter can increase the heating load. These two different purposes of ventilation can be achieved using regulated or adaptive ventilation systems. However, most residential buildings with natural ventilation keep their vent configuration and ratios constant throughout the year. In such roof systems, attic ventilation rates vary with the driving forces buoyancy, and wind pressure. Roodvoets [1] attempted to develop a protocol to determine the driving forces to add additional ventilation during retrofitting in mixed climates. He suggested that a wind speed of five metres per second is considered to be sufficient ventilation to remove all the unwanted moisture accumulated in the residential occupied space. Forest and Walker [2] measured the ACH (air exchange per hour) values for attics with an intentional venting area and for sealed attics at the research houses at the University of Alberta. Their findings showed a ventilation rate varying from 0 to 50 ACH for the attic with a venting area of 1:300 ratio to the attic floor. Measurement results by Morrison Hershfield for ventilation rates using tracer gases lie in a range of 1 to 5 ACH. Lstiburek recommended that the air change in a perfectly built and vented attic (1:300 ratio) should result in an average air change rate of 3 to 6 ACH [3]. In the current attic thermal and hygrothermal simulation practice, researchers and designers pick a constant ventilation rate from the proposed ranges or dynamically calculate the attic ventilation rates using an airflow network model and the prevailing driving forces. Both these approaches consider the attic to have mixed air space with uniform temperature and humidity distribution, which in reality is not the case. This approach lacks to provide detailed information on the attic heat-air-moisture transport, including possible moisture distribution differences along the length of the sheathing and temperature in the attic space. Such information can be important for identifying areas in the attic roof where moisture damage risk is expected to be higher and where extreme temperatures that may affect the roof durability.

In this study, computational fluid dynamics (CFD) is used to map the temperature and airflow patterns in attic roofs under buoyancy and wind-induced driving forces. The analysis is carried out using COMSOL Multiphysics[1] and considering a two-dimensional (2D) attic roof geometry that includes the soffit and the baffle regions as part of the computational domain. Temperature profiles are investigated for the attic air space and the roof sheathing on typical winter and summer days in cold and mild climates, which are represented by Ottawa and Vancouver, respectively. The CFD results are used to quantify the attic ventilation rates that are expected for buoyancy and wind-driven flow cases. In addition, the simulation results are used to develop a relationship between attic ventilation rates (ACH) and solar radiation for both winter and summer conditions. The effect of attic ventilation on heating and cooling loads is also assessed by considering different ventilation scenarios. Finally, the hygrothermal performance of the attic roof sheathing in a cold climate (Prince George) both with and without ceiling air leakage and with different attic insulation thicknesses is studied by coupling the CFD model and the benchmarked hygrothermal model, HAMFit [4].

In the next sections, first, the COMSOL Multiphysics CFD mathematical models used in this study are presented along with a benchmark exercise. Then the physical description of an attic roof considered in the research and the procedures that are followed for an optimum computational model are discussed. Finally, results obtained from the CFD and hygrothermal analysis are given in sequence.

[1]http://www.comsol.com/

2. Mathematical Model

Figure 1 illustrates the typical thermal loads on an attic system and the openings for air exchange. Due to the different thermal loads on the roof, ceiling, and incoming air, the airflow in the attic is non-isothermal. Thus, the energy and momentum balance equations for the air in the attic space need to be solved, along with the conduction heat transfers through the attic floor layers and roof structures. Such type of heat transfer and fluid flow problem is defined as a conjugate heat transfer. In Section 2.1, the governing equations that are used to solve the temperature and airflow field in the attic space and accompanying structures are described.

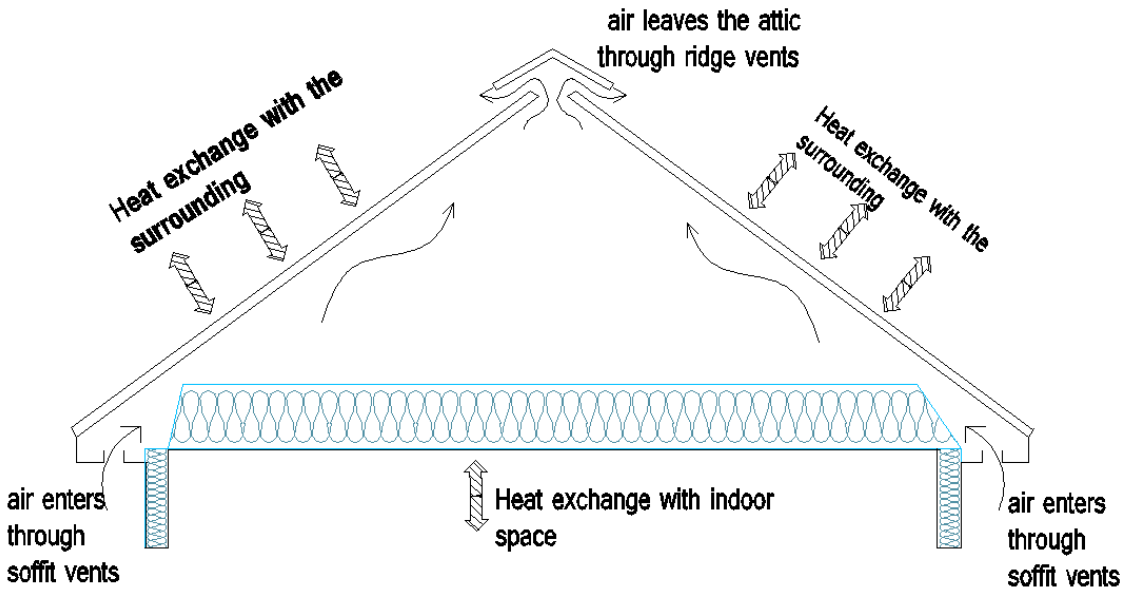

Figure 1. Schematic diagram of heat exchange and airflow in a simplified attic system

2.1 Governing Equations

The fluid flow in the attic can be characterized as an incompressible flow. The governing equations for the mass, momentum and energy conservation in a two-dimensional flow are given in Equation 1, Equation 2 and Equation 3, respectively. These momentum equations, which can also be referred to as Reynolds-Average Navier-Stokes (RANS) equations, are derived from the general Navier-Stokes equations after applying Reynold averaging technique. Thus, in the equations, *u*, *v*, and *T*

are mean values of x- and y-velocity components, and temperature and μ is the dynamic viscosity of air. The Reynolds stresses are modeled analogues to shear stresses using eddy viscosity (μ_T). The flow in the attic can be mixed flow, where both forced and buoyancy-driven flows can coexist. To capture the buoyancy-driven flow, the Boussinesq approximation is applied into the RANS momentum equation in the y-direction. This effectively assumes constant density (ρ^o) in all terms except the body force and thereby introduces a buoyancy term, $g(\rho - \rho^o)$, in the momentum balance equation, in which g is the gravitational acceleration and ρ is temperature-dependent density, which is calculated based on ideal gas law.

$$\frac{\partial u}{\partial x} + \frac{\partial v}{\partial y} = 0 \tag{1}$$

$$\rho^o \left(\frac{\partial u}{\partial t} + u\frac{\partial u}{\partial x} + v\frac{\partial u}{\partial y}\right) = -\frac{\partial p}{\partial x} + (\mu + \mu_T)\left(\frac{\partial^2 u}{\partial x^2} + \frac{\partial^2 u}{\partial y^2}\right) \tag{2}$$

$$\rho^o \left(\frac{\partial v}{\partial t} + u\frac{\partial v}{\partial x} + v\frac{\partial v}{\partial y}\right) = -\frac{\partial p}{\partial y} + (\mu + \mu_T)\left(\frac{\partial^2 v}{\partial x^2} + \frac{\partial^2 v}{\partial y^2}\right) + g(\rho - \rho^o)$$

$$\rho^o C_p \left(\frac{\partial T}{\partial t} + u\frac{\partial T}{\partial x} + v\frac{\partial T}{\partial y}\right) = (\lambda + \lambda_T)\left(\frac{\partial^2 T}{\partial x^2} + \frac{\partial^2 T}{\partial y^2}\right) \tag{3}$$

The turbulent model used in this report is the *k*-*ω* two-equation eddy viscosity turbulent model. This model is found to be robust for isothermal and non-isothermal flows in an enclosed space [5]. In this model, the eddy viscosity is defined as $\mu_T = \rho\frac{k}{\omega}$, where *k* is the turbulent kinetic energy and *ω* is the dissipation per unit turbulent kinetic energy. The eddy conductivity, λ_T, in the energy balance equation is defined by the turbulent Prandtl number and eddy viscosity values $Pr_T = C_p\frac{\mu_T}{\lambda_T}$; here, C_p is the specific heat of air. The governing equations for *k* and *ω* and the Kays-Crawford equation for the turbulent Prandtl number, which are implemented in the COMSOL Multiphysics and used in this work, are given in Equations 4, 5 and 6, respectively. The accompanying coefficients are shown in Table 1. The heat transfer through solid components of the attic structure is computed by setting *u*, *v* and λ_T values to zero in the energy balance equation, Equation 3.

$$\rho^o\left(\frac{\partial k}{\partial t}+u\frac{\partial k}{\partial x}+v\frac{\partial k}{\partial y}\right)=(\mu+\mu_T\sigma_k^*)\left(\frac{\partial^2 k}{\partial x^2}+\frac{\partial^2 k}{\partial y^2}\right)+P_k-\rho^o\beta_0^* k\omega \quad (4)$$

$$\rho^o\left(\frac{\partial \omega}{\partial t}+u\frac{\partial \omega}{\partial x}+v\frac{\partial \omega}{\partial y}\right)=(\mu+\mu_T\sigma_\omega^*)\left(\frac{\partial^2 \omega}{\partial x^2}+\frac{\partial^2 \omega}{\partial y^2}\right)+\alpha\frac{\omega}{k}P_k-\rho\beta_0\ \omega^2 \quad (5)$$

where $P_k=\mu_T[\nabla u:(\nabla u+(\nabla u)^T]$

$$Pr_T=\left(\frac{1}{2Pr_{T_\infty}}+\frac{0.3}{\sqrt{Pr_{T_\infty}}}\frac{C_p\mu_T}{\lambda}-\left(0.3\frac{C_p\mu_T}{\lambda}\right)^2(1-e^{-\lambda/(0.3C_p\mu_T\sqrt{P_{r\infty}})}\right)^{-1} \quad (6)$$

where Prandtl number at infinity is $Pr_{T_\infty}=0.85$ and λ is conductivity.

Table 1. The k-ω turbulent model coefficients used in the model

Coefficient	Value	Coefficient	Value
α	0.52	β_o^*	0.09
σ_k^*	0.5	k_v	0.41
σ_w	0.5	B	5.2
β_o	0.072		

The conjugate heat transfer model is used to describe heat transfer in solids and non-isothermal flow in fluids. The heat transfer module is tightly coupled with the turbulent fluid flow model and described in Equation 3. In addition to conduction and convection, the surface-to-surface radiation exchange between the inner surface of the roof sheathing and the top surface of the ceiling insulation are considered in this report.

3. CFD Model Benchmarking

Most unvented attic experimental and numerical simulation models assume a shape of an isosceles triangle, with the two inclining sides representing the roof while the horizontal side symbolizes the ceiling. Flack et al. [6] conducted an experimental measurement of turbulent natural convection in an attic-like shape with temperature variation from below. The buoyancy flow inside the triangular shape was visualized using Schlieren and laser velocimetry tools.

In this report, the velocity and temperature profiles in the triangular enclosure reported by Flack [6, 7] are used for benchmarking of the CFD model presented in the previous section. This three-sided enclosure can seamlessly represent the sealed attic model used in this report.

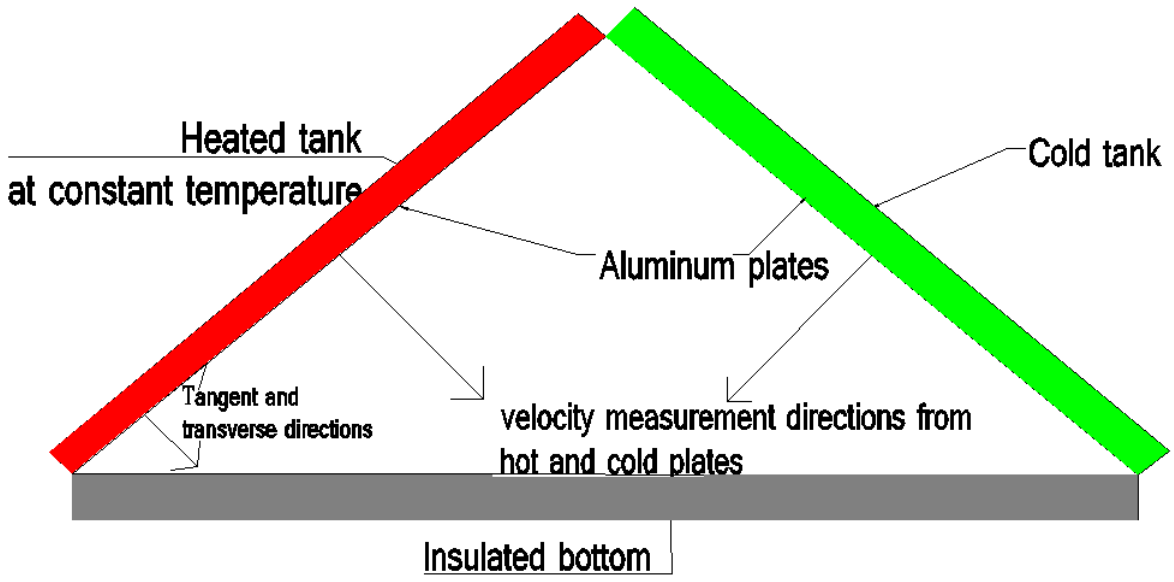

Figure 2. Flank and Witt's experimental setup

In his experiment, Flack used an air-filled triangular enclosure built from two constant temperature tanks and one horizontal insulated bottom, as shown in Figure 2. A Wollaston prism Schlieren interferometer was used to measure the heat transfer rates in the same enclosure. Polished aluminum plates were used to form the two inclined sides of the triangular enclosure. Two-dimensional velocity profiles, in tangent and transverse directions of the inclined plane, were measured using Laser Velocimeter. The inclined surfaces are subjected to hot temperatures on one side and cold temperatures on the other side. Figure 3 presents the Laser Velocimeter

measurements of velocity profiles in a perpendicular direction from the hot and cold plates at midpoints of the isothermal inclined surfaces, along with the CFD simulation results of the corresponding locations. In this experiment [6], the hot and cold temperatures of the inclined plate are set at a constant temperature of 64°C and 0°C, respectively. Eta (η) and U are normalized space and velocity values that are defined as a function of directions normal and tangential to the isothermal surface, the length of the isothermal surface, Grashof's number, and average velocity.

$$\eta = \frac{Y}{(4X)^{\frac{1}{4}}} \text{ where } Y = \frac{Gr^{1/4}y}{L} \text{ and } X = \frac{x}{L} \tag{7}$$

$$U = \left(\frac{Gr}{4X}\right)^{2} \bar{u}$$

where *x* and *y* are tangent and normal directions to an isothermal surface;

Gr is Grashof's number;

L is the length of the isothermal surface;

$\bar{u}$ is normalized velocity.

As can be seen in Figure 3, the model predictions are in good agreement with the experimental measurements. The maximum root mean square error (RMSE) between the measurement and simulation results is only 2.1%.

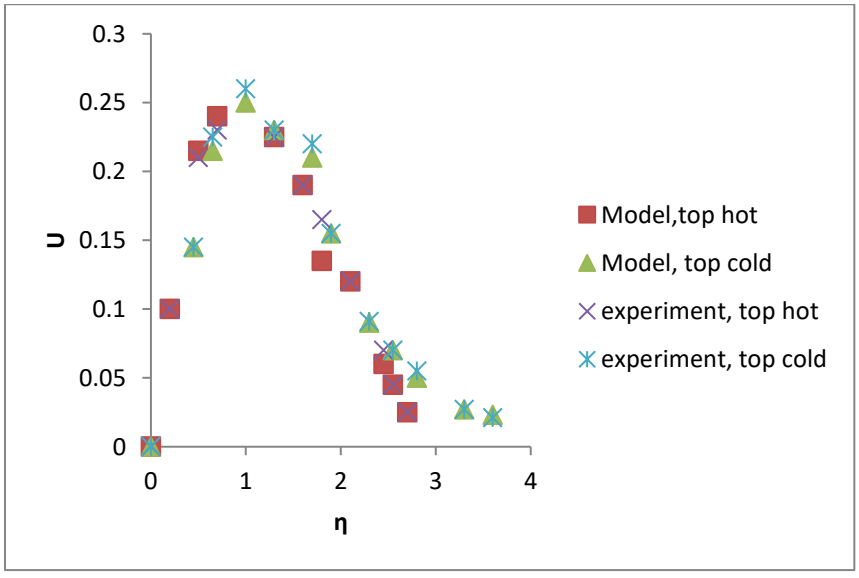

Figure 3. Comparison of the predicted and experimentally measured velocity profile

As an additional model validation exercise, two experimental cases with boundary conditions that give different velocity and temperature distributions are considered. The experiments are done by Flanks [7] using the experimental setup discussed above. In one of the experiments, the horizontal plate is kept at 20^{o}C and the inclined plates are kept at 40^{o}C, which is referred here as the 'top hot' case. In the second one, the inclined plates are maintained at 0^{o}C and the horizontal plate at 20^{o}C, which is referred here as the 'top cold' case. The experimentally measured temperature distributions along the centerline of the triangular enclosure in the two experiments are normalized and shown in Figure 4. For comparison purposes, the normalized CFD simulation results are superimposed on the same figure. As can be seen in the figure, the CFD simulation results agree very well with the measured data.

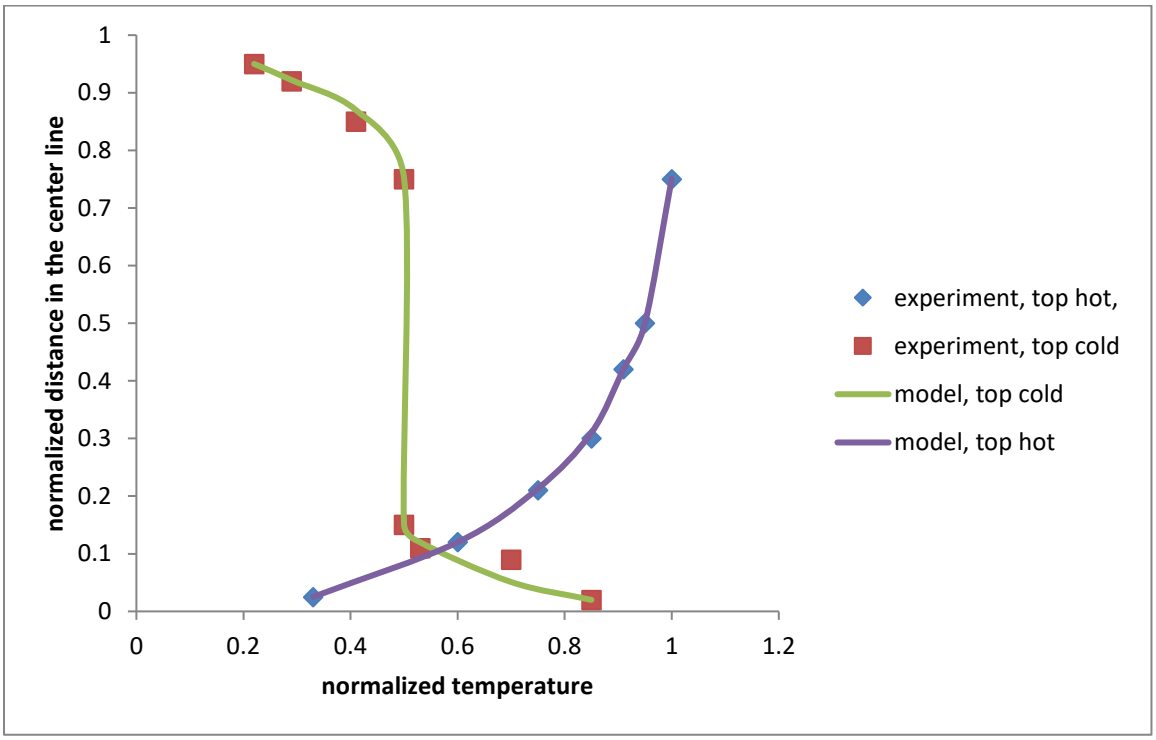

Figure 4. Comparison of CFD predictions and experimentally measured temperature values

4. Physical Model

In this report, a sloped roof with a 4:12 pitch and an attic floor area of 74.32 m^2 (800 ft^2) is considered for the study (see Figure 5). According to the Canadian National Building Code [8] (NBC 2015), roofs with insulation between the interior ceiling and roof sheathing require ventilation. For the roof system considered here, the design attic ventilation opening area is set to be 1/300 of the attic floor area. Accordingly, the roof with an attic floor area of 74.32 m^2 (800 ft^2) will need to have a 0.25 m^2 (2.7 ft^2) area of opening for ventilation to satisfy the Code requirement. The Code also requires the roof to have equal vent opening areas on the opposite side of the roof space, and the ventilation openings at the top and bottom of the roof space each to be over 25% of the total ventilation area. The common design practice is to allocate 60% of the ventilation opening at the bottom (soffit) and 40% at the top (ridge) of the roof space. In this report, following the current practice, the soffit and ridge vent opening areas are assumed to be 0.15 m^2 (0.075 m^2 per side) and 0.09 m^2, respectively, which are equivalent to having 10 mm and 15 mm continuous openings at the soffit and ridge level as presented in Figure 5. To prevent the insulation from blocking airflow at the bottom of the roof, a baffle with 51 mm depth and 91 mm long is placed between the sheathing and the insulation. The attic system considered in the study focuses on existing houses. Hence, in this work, the attic is assumed to be that of an existing house and insulated according to the 1997 Model National Energy Code of Canada [9] (MNECC): 211 mm depth of loose cellulose insulation of RSI 5.3 (R-30) at the center and 97 mm at the eave edge. The attic floor is drywall with 6 mil polyethylene sheet as a vapor and air barrier on top, and the roof deck is built with shingles, roof underlay, and plywood sheathing. The polyethylene and sheathing membranes are not shown in Figure 5. The thermal conductivities and heat capacity of the drywall, insulation, and plywood sheathing are given in Table 2. The solar absorptivity and emissivity properties of the roof shingles are 0.8 and 0.9, respectively.

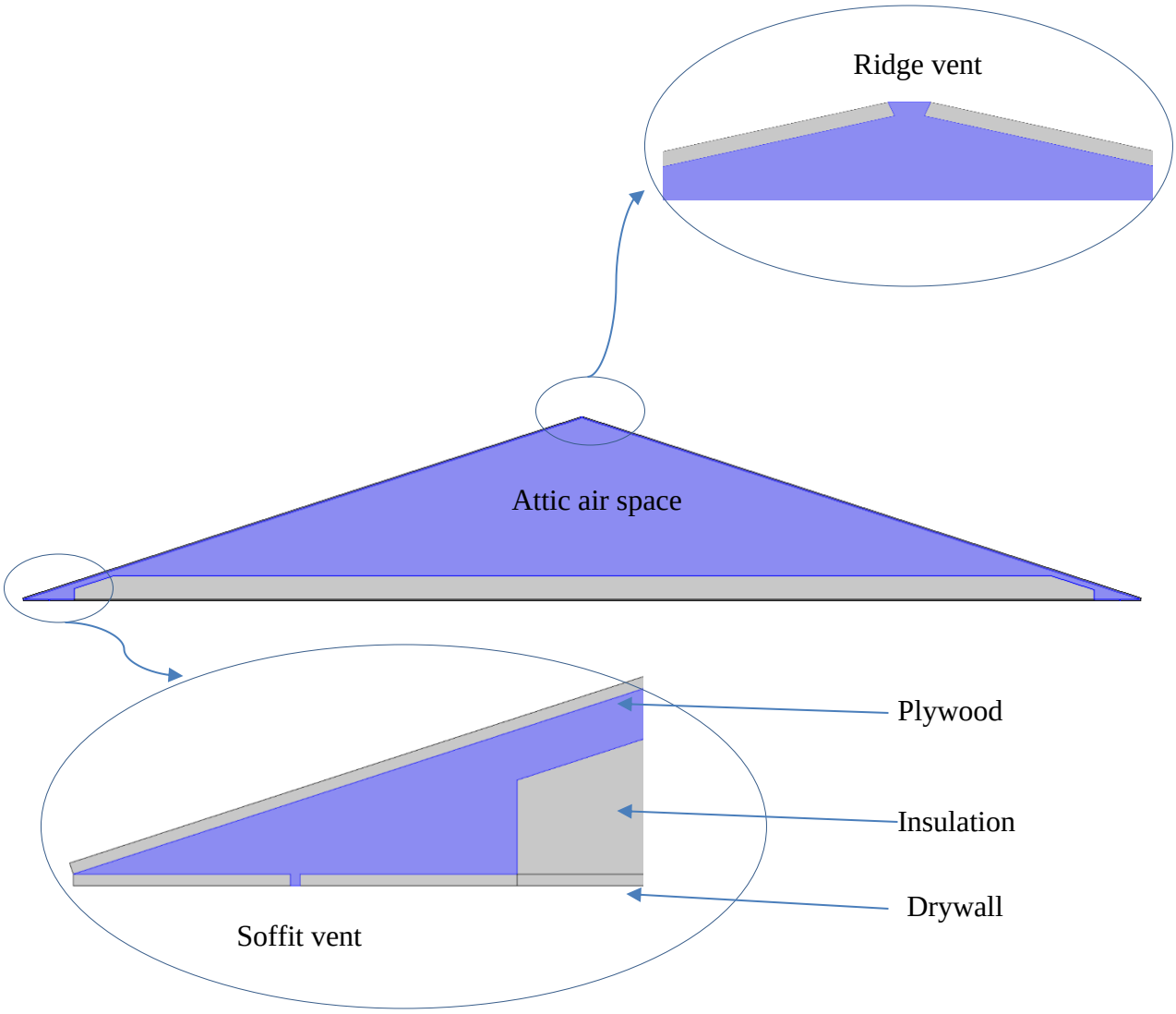

Figure 5. Physical model of attic roof considered in the study

Table 2. Thermal conductivity and heat capacity of the attic roof layers

	Thickness (m)	Thermal conductivity (W/(m.K))	Heat capacity (J/(kg.K))
Drywall	0.0125	0.177	1097
Loose Cellulose Insulation	0.211	0.04	1007
Plywood	0.0125	0.13	1507

5. CFD Simulation Setup

The physical attic roof model shown in Figure 5 is drawn in the COMSOL GUI and forms the computational domain. The computational domain is discretized with triangular finite elements mesh and solved with time-dependent solver, as the boundary conditions considered in this report are time-dependent. The implicit time-stepping scheme uses the Backward Differentiation Formulas (BDF) method to update the solutions in time.

5.1 Mesh Sensitivity Check

A user-controlled mesh is created, and sizes and types of grids are developed for different regions of the computational domain to allow COMSOL to solve the model accurately and economically. The attic space has a finer mesh size as compared with the solid parts of the attic, such as drywall, roof sheathing, and insulation. This approach increased the modeling accuracy because the fluid dynamics model demands a finer mesh size. Regions around the inlet and the outlet vents are meshed with extra fine mesh sizes as they are relatively small in size, and air-jet enters and leaves the system at these ports with a relatively high velocity. In addition, boundary layer meshes are envisaged near the solid boundaries, and corner refinement meshes are included at corners of the fluid flow boundary.

To make sure an optimal mesh size (beyond which the solution accuracy does not improve significantly and becomes mesh size-independent) is used in the modeling, a mesh size sensitivity test is conducted by comparing the results of three models with a different number of elements. The mesh sizes used for comparison were 21,256 elements, 43,675 elements and 76,312 elements. The first two models' mass flow rate, average attic temperature value, and processing time are compared with the densest mesh model. In comparison to the model with ~76,000 element, the model with 43,675 elements has a small mass flow rate and average attic temperature differences (1.89% and 1.34%, respectively) when compared with the model with 21,256 elements. This can be considered as a very small difference for a model with almost half of the number of mesh elements. The computational time saved by using 21,256 elements compared to 43,675 elements is marginal. This outcome prompted the use of an attic model consisting of 43,675 elements throughout this study. These findings are tabulated in Table 3.

Table 3. Percentage error and percentage time saved by different mesh sizes

Mesh size	% difference compared to most dense mesh size (76,312 elements)		% time saved compared most dense mesh size (76,312 elements)
	Mass flow rate	Avg. Attic temperature	
21,256 elements	2.73	2.01	16.14
43,675 elements	1.89	1.34	17.35

5.2 Boundary Conditions

The problem in this study involves an attic enclosure exposed to variable thermal loading. It also includes inlet vents that allow an air jet to enter into the attic space by wind pressure or stack effect and outlet vents to remove air from the attic. These boundary conditions are used by the coupled fluid flow (Navier -Stokes) and heat transfer (energy balance) mathematical models. The boundary conditions are generated based on Ottawa and Vancouver weather data, which represent locations with cold winter and hot summer days and mild temperature conditions as the interior and the coastal regions of British Columbia.

To assess the temperature and airflow (ACH) conditions in the attic roof during day and night times of a typical winter and summer day, hourly temperature data are constructed using Ottawa's January and July monthly averages and maximum temperature differences following the ASHRAE Fundamentals (2013) [10] procedure for generating design day data. The same procedure is applied for Vancouver but using August instead of July for the summer period. In Figure 6 and Figure 7, the hourly temperature and the global horizontal solar radiation data for Ottawa and Vancouver, respectively, are presented. The solar radiations on the roof surface are calculated based on their orientations and inclinations.

Considering a building with its ridge running from north to south, the left and the right sides of the attic roof model (Figure 5) represent the roof parts facing east and west, respectively. In the simulations, the east and the west roof surfaces receive different solar radiations that vary hourly. The variable thermal loads on the roof are calculated as a composition of heat flux terms from

convection heat transfer, longwave radiation exchange and solar radiation values. The heat flux values at the left and right side of the roof are equated as:

$$Q_l = h_{out}(T_{out} - T) + \alpha Solgain_L$$
$$Q_r = h_{out}(T_{out} - T) + \alpha Solgain_R \quad (7)$$

where

Q_l: heat flux on the left side of the roof

Q_r: heat flux on the right side of the roof

h_{out}: outside heat transfer coefficient

T_{out}: outside temperature

T: attic temperature

$Solgain_L$: solar radiation on the left side of the roof

$Solgain_R$: solar radiation on the right side of the roof

α: Solar absorption coefficient of the outside surface of the roof shingles

The first term in the left-hand side represents the combined effects of the convective and longwave radiation heat transfers using an equivalent surface transfer coefficient, h_{out}

Similarly, the heat transfer between the indoor space and the ceiling is represented by Equation 8.

$$Q_c = h_{in}(T_{in} - T) \quad (8)$$

where:

Q_c: heat flux passes through the ceiling

h_{in}: internal surface coefficient

T_{in}: conditioned space temperatures

In this work, the conditioned space temperature is set to 21^{o}C, and heat transfer coefficient values of 25 W/(m^2.K) and 8 W/(m^2.K) are used for the exterior and interior surfaces, respectively.

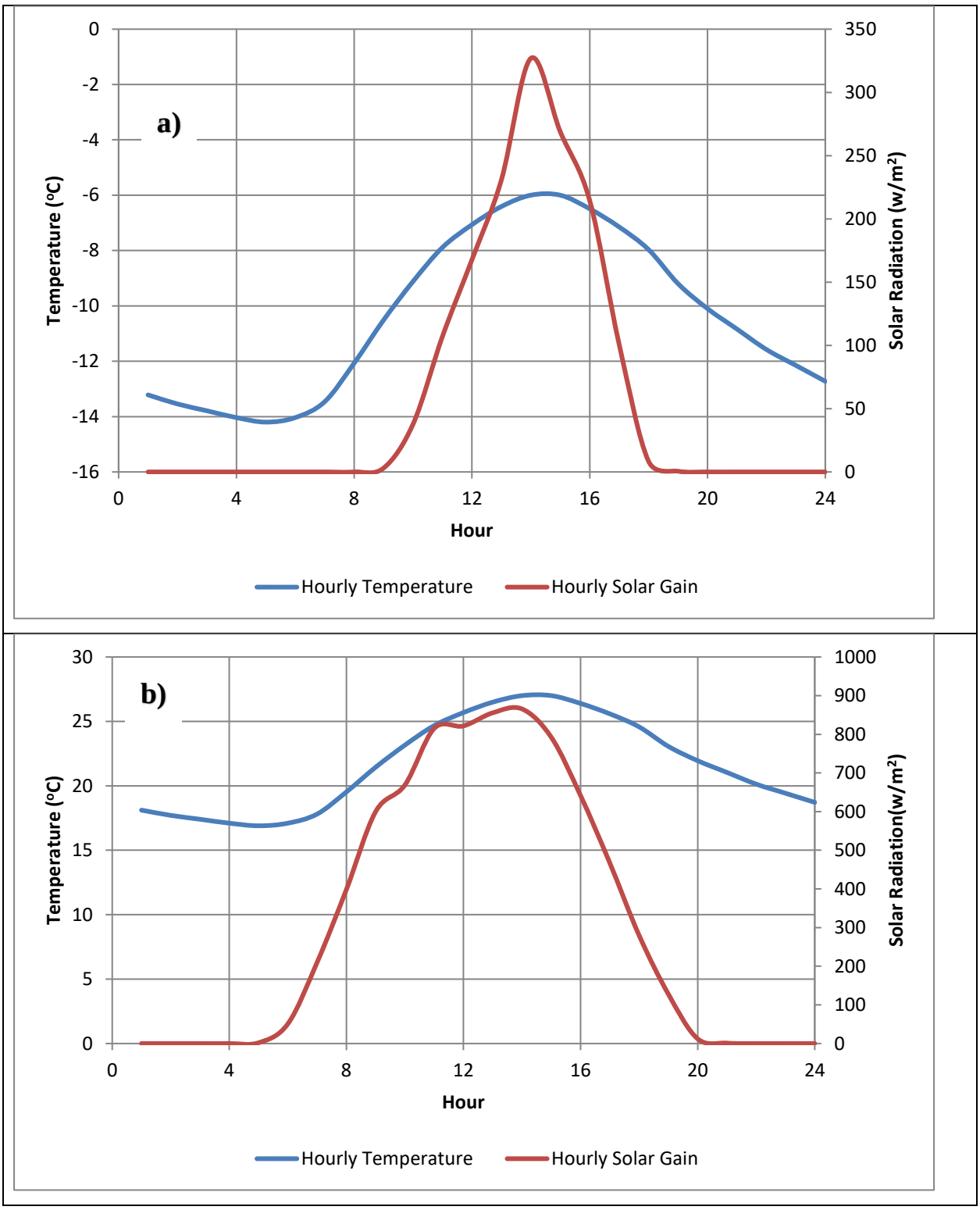

Figure 6. Hourly temperature and solar radiation profiles in a typical winter (a) and summer (b) day in cold winter and hot summer location (Ottawa), respectively

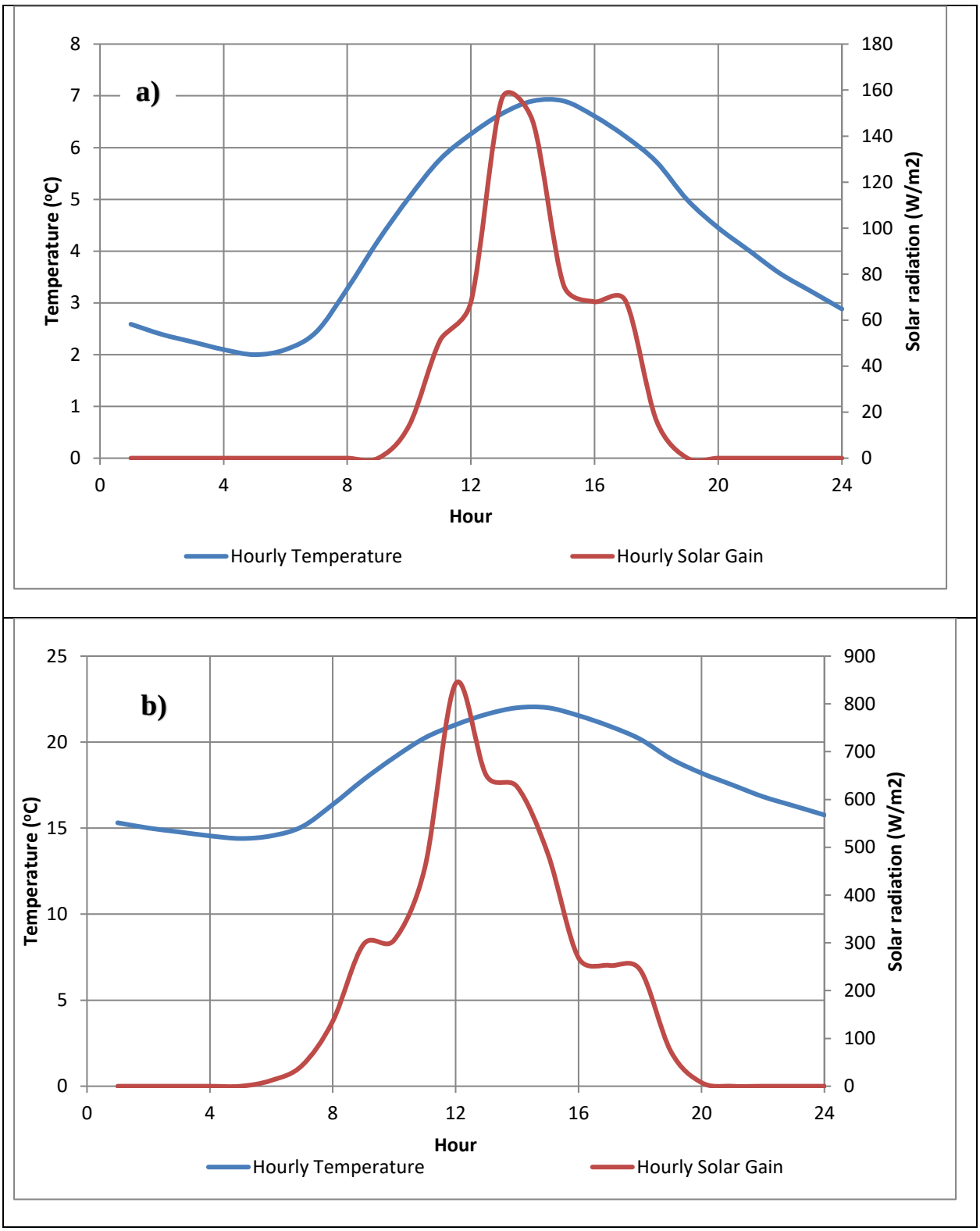

Figure 7. Hourly temperature and solar radiation profiles in a typical winter (a) and summer (b) day in mild climate (Vancouver), respectively

For airflow calculation, pressure boundary conditions are applied at the soffits and ridge openings. The surface pressures are calculated from the local pressure coefficients and wind speed at roof level, using Equation 9. In this work, the local pressure coefficients from ASHRAE Fundamentals (2013) [10] are used. Accordingly, pressure coefficient values of 0.8 and -0.43 are used at the windward and leeward soffit openings, respectively, and a pressure coefficient of -1 is used at the ridge opening. In this study, two wind speed conditions, a moderate (1.8 m/s) and a low (1 m/s) wind speed, are considered based on the Building Science Centre of Excellence wind speed measurement results. The corresponding dynamic pressures $\left(\frac{\rho {U_r}^2}{2}\right)$ at the roof height are 2 Pa and 0.6 Pa, respectively. In simulation cases with no wind pressure, the pressure boundary conditions at all openings will be atmospheric pressure and defined as a gauge pressure of 0 Pa.

$$p_s = Cp_l \frac{\rho {U_r}^2}{2} \qquad (9)$$

Where p_s is surface pressure; Cp_l local pressure coefficient; U_r wind speed at roof height and ρ air density.

6. Results and Discussion

In this section, first the airflow and temperature patterns in the attic space, as well as the heat transfer through the attic floor during typical cold winter and hot summer days are presented for cases of four different venting scenarios. The corresponding simulation results for the mild Vancouver weather is shown in Appendix A. Then after, the hygrothermal response of the attic roof sheathing in a cold climate (Prince George) is presented.

In the first scenario, the attic is sealed, and there are no inlet and outlet vents. In the second scenario, attic ventilation takes place due to buoyancy only. In the third and fourth scenarios, wind-driven ventilation is investigated at 2 Pa and 0.6 Pa. The wind is assumed to blow from east to west (left to right in Figure 5). For the last three scenarios, the contribution of solar-driven attic ventilation during a typical winter and summer day are presented.

6.1 Temperature and Airflow Distributions in Attic Space

Natural convection flow in the attic can be generated from the insulation top surface or underside of roof sheathing, depending on their temperature. Although these situations, in general, correspond to winter and summer cases, sheathing temperature can be significantly higher than the top of the insulation surface during the winter period due to heating up by solar radiation. The Grashof's numbers for the four simulation cases during the night (no solar radiation) and 2:00 pm (when there is solar radiation) are presented in Table 4. The length of the rafter and the roof height are used as characteristic lengths for calculation of Grashof's number for the cases with and without solar radiation, respectively. As can be seen from the table, the Grashof numbers in all cases are higher than 2.5E+8, and consequently, the flows are near turbulent or fully turbulent.

Table 4. Grashof's numbers of the four simulation cases at different conditions

Attic ventilation scenarios	Winter		Summer	
	12:00 AM (no solar radiation)	2:00 PM (with solar radiation)	12:00 AM (no solar)	2:00 PM (with solar radiation)
Sealed attic	2.0E+9	7.5E+11	4.6E+8	1.5E+12
Buoyancy only	2.5E+9	1.3E+12	2.5E+8	2.8E+12
Wind pressure at 0.6 Pa	1.2E+9	1.5E+12	2.5E+8	3.0E+12
Wind pressure at 2 Pa	1.2E+9	1.7E+12	3.2E+8	3.3E+12

The temperature and airflow fields in an attic at midnight with different ventilation scenarios are shown in Figure 8. The results represent conditions on a winter day with no solar radiation. Although the temperature contour plots are similar, the airflow patterns are quite different. In the attic case with 2 Pa wind pressure (Figure 8, d), the incoming air seems to have enough momentum to flow along the underside of the sheathing to the ridge outlet. As the wind pressure is reduced to 0.6 Pa (Figure 8, c), the incoming cold air stream loses its inertia and changes course and flows over the insulation surface and underside of the opposite roof sheathing by buoyancy action before exiting at the ridge opening. When there is no wind pressure, the buoyancy force creates a

symmetrical airflow pattern in the vented attic space, with relatively warm air existing along the symmetry line (Figure 8, b). In the sealed attic, two flow regions with different sizes are created (Figure 8, a). Figure 9 shows the temperature and airflow patterns in the attic spaces of the four attic ventilation scenarios at 2:00 pm of a winter day with solar radiation. As can be seen in Figure 9, the airflows in all cases are primarily due to a solar-driven buoyancy force, which draws air to flow along the underside of the solar-heated sheathing, including the case with a wind pressure of 2 Pa (Figure 9, d). There are notable flow pattern differences at 12:00 am (Figure 8) and 2:00 pm (Figure 9). The cold air stream with 2 Pa (Figure 9, d) wind pressure doesn't flow near the left roof sheathing as in Figure 8 (d); instead, it is forced to change its flow path and exit after flowing under the heated sheathing (right side). The airflow in the sealed attic, in Figure 8 (a), has changed from two flow regions to one in Figure 9 (a). Simulation results of the four attic operation scenarios on a summer day yielded similar airflow patterns.

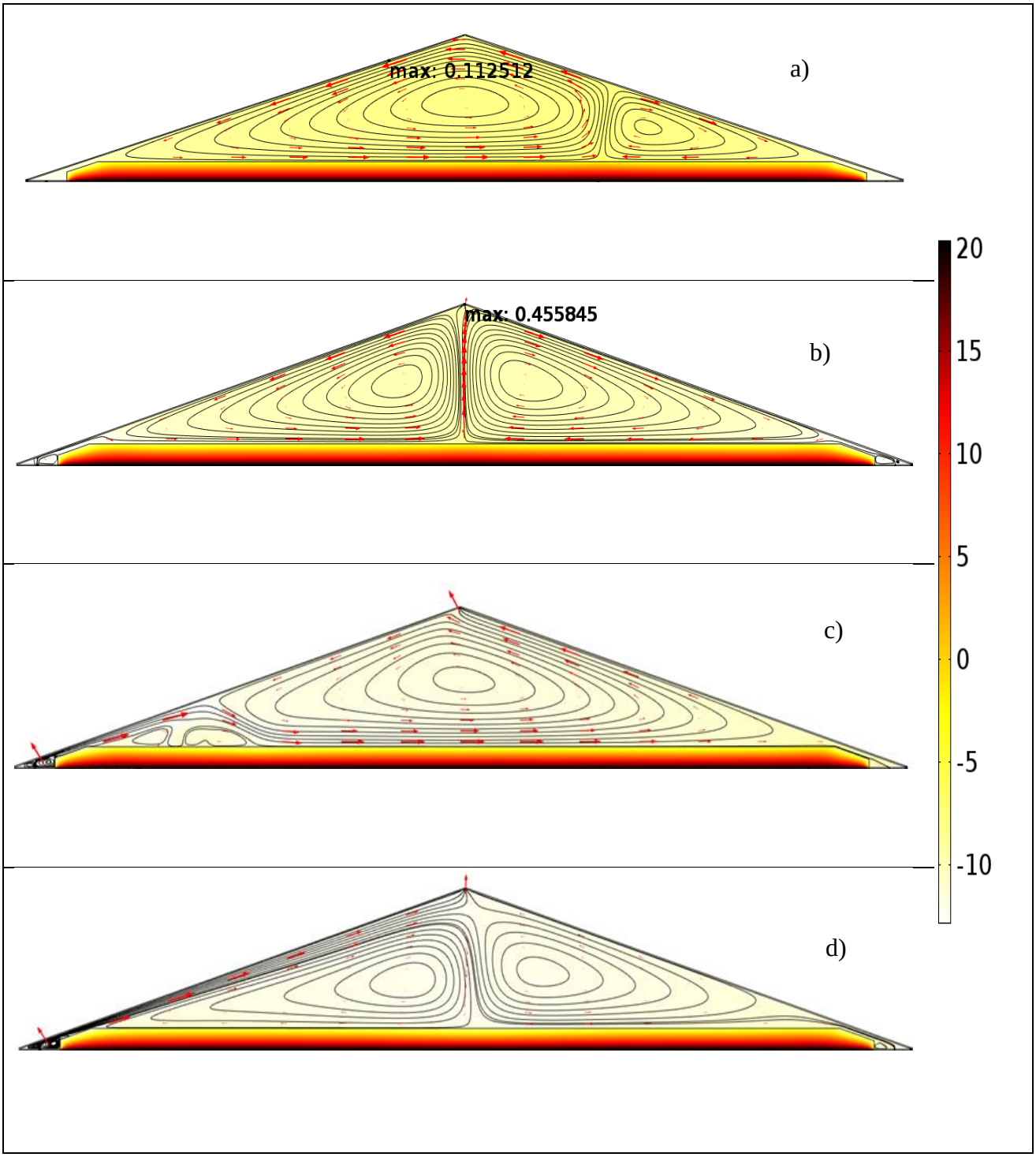

Figure 8. Temperature and airflow fields for different attic ventilation scenarios: (a) sealed attic, (b) stack-effect, (c) 0.6 Pa wind pressure and (d) 2 Pa wind pressure—a case for winter day at 12am (Ottawa)

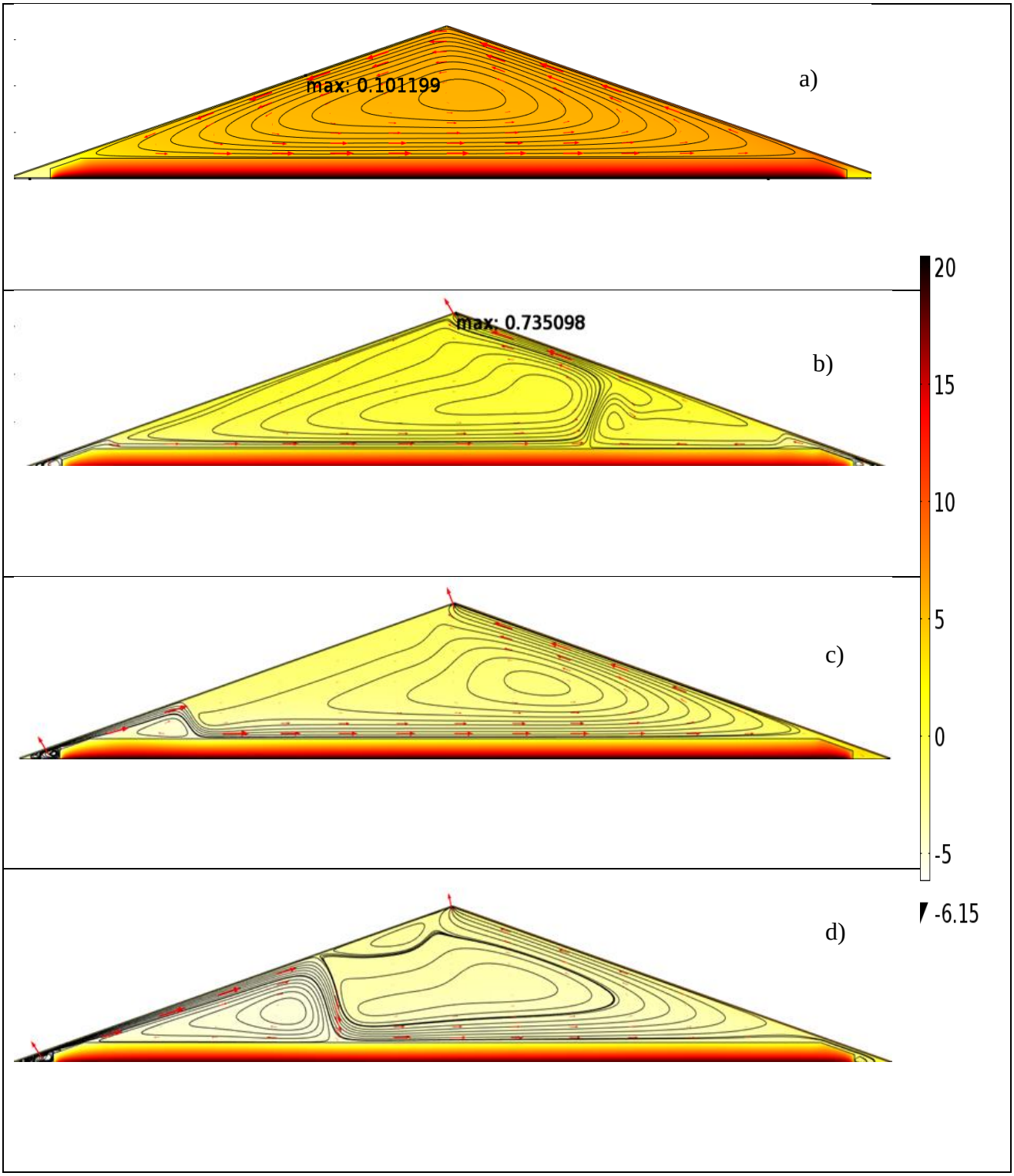

Figure 9. Temperature and airflow fields for different attic ventilation scenarios: (a) sealed attic, (b) stack-effect, (c) 0.6 Pa wind pressure and (d) 2Pa wind pressure—a case for winter day at 2:00 pm with solar radiation (Ottawa).

6.2 Attic Air and Roof Surface Temperature

The average attic air temperatures during winter and a summer day for the four attic operation scenarios are shown in Figure 10. As can be seen in the figures, during both winter and summer days, the attic air temperature is the highest in the sealed attic and the lowest in the wind-ventilated cases (2 Pa wind pressure). The temperature differences increase with solar radiation and reach a maximum of 10°C and 17°C in the winter and summer days, respectively. The warmer attic temperature (cases of the sealed attic) can be good during the winter period as it reduces heating load, and a disadvantage during the summer period as it increases cooling load. The opposite is true for the highly ventilated attic roof.

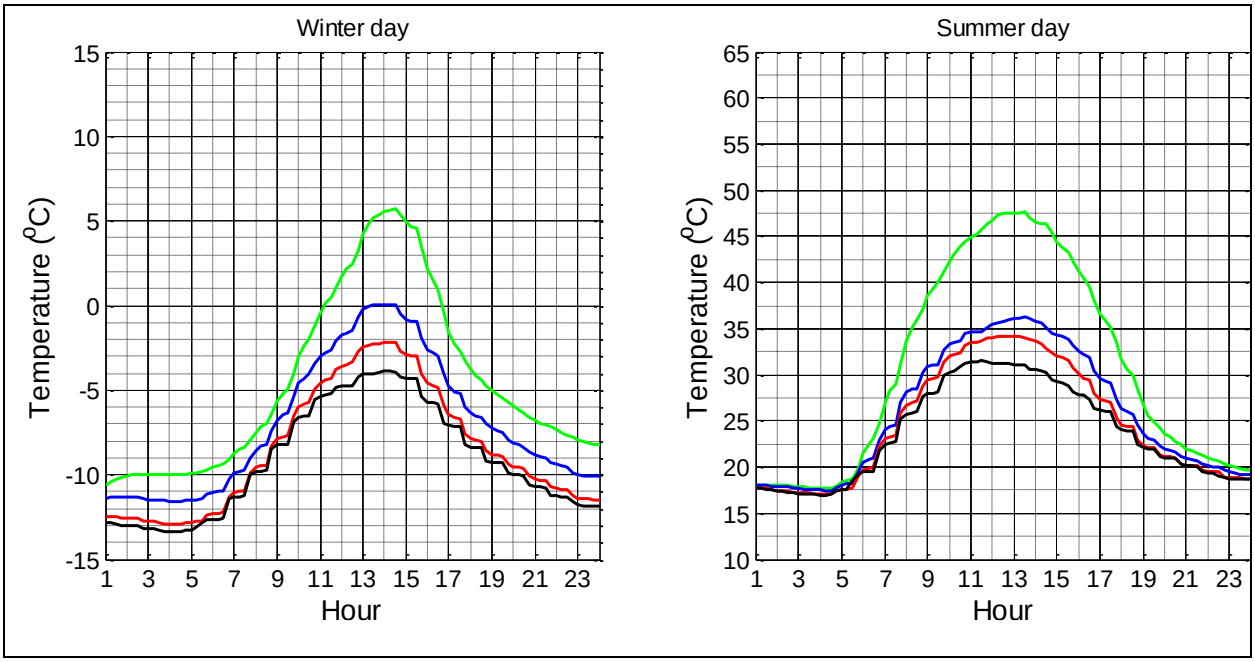

Figure 10 Average attic air temperature for different attic ventilation scenarios during a typical winter and summer day (Ottawa). Color code: green (sealed), blue (stack effect), red (0.6 Pa wind pressure), black (2 Pa wind pressure)

The maximum temperature of the roof sheathing during the winter and summer days considered in this study are shown in Figure 11. As can be seen in the figures, there is no significant sheathing temperature difference between the four scenarios. The daily temperature fluctuations during the winter and the summer days are about 23°C and 43°C, respectively. These high daily temperature fluctuations can have an impact on the service life of the roof shingles.

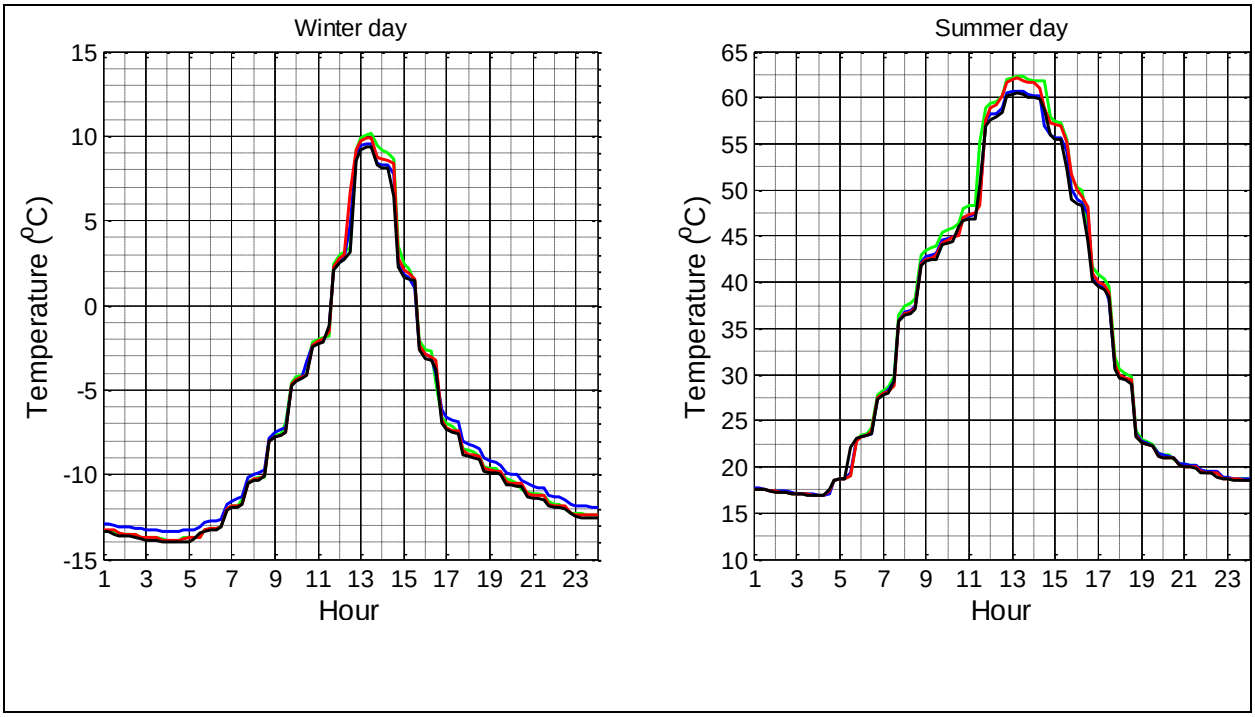

Figure 11. Maximum roof sheathing temperatures for different attic ventilation scenarios during a typical winter and summer day (Ottawa). Color code: green (sealed), blue (stack effect), red (0.6 Pa wind pressure), black (2 Pa wind pressure)

6.3 Attic Ventilation Rates

The amount of attic ventilation expected in typical winter and summer days under different wind conditions are presented in Figure 12. In the absence of wind and solar radiation, buoyancy-induced ventilation yields about 4 ACH during the winter and 1.5 ACH in the summer. As shown in Figure 13, attic air change per hour increases as solar radiation increases. For the same solar radiation, the ACH in the winter is higher than in the summer, which must be attributed to the enhanced buoyancy flow due to higher temperature differences in the winter. For the boundary conditions considered in this report, the total air change per day in the winter is about 10% higher than in the summer, and in both cases, the highest ventilation rates are under 7 ACH. In the scenarios where the attic is exposed to 0.6 Pa and 2 Pa wind pressure, the ventilation rate in the winter increases by 2.5 and 5.0 times, respectively, the scenario with no wind pressure (only stack effect), Figure 12. The wind-induced ventilation rates during the winter and summer days are nearly the same: 9–10 ACH and 19–20.5 ACH for the case of 0.6 Pa and 2 Pa wind pressure, respectively. The nearly constant ventilation rate shown in Figure 12 suggests that, unlike the stack-only ventilation scenario, the wind induced ventilation is less sensitive to solar radiation.

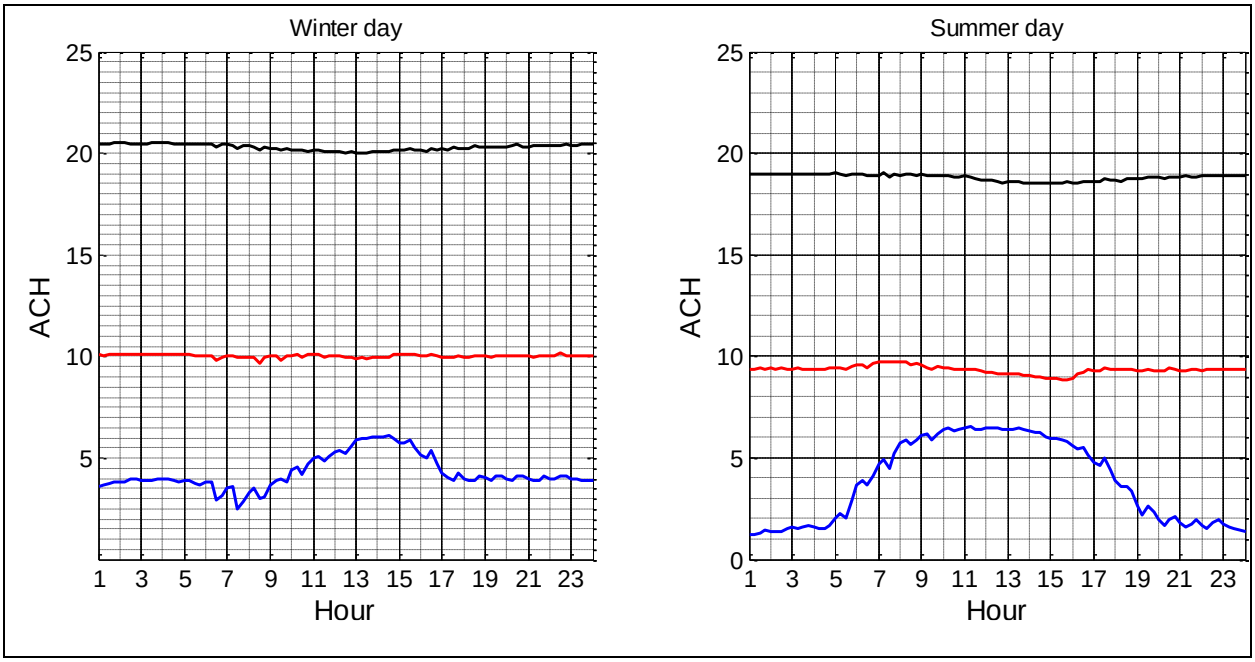

Figure 12. Attic ventilation rates for different attic ventilation scenarios during a typical winter and summer day (Ottawa). Color code: blue (stack effect), red (0.6 Pa wind pressure), black (2 Pa wind pressure)

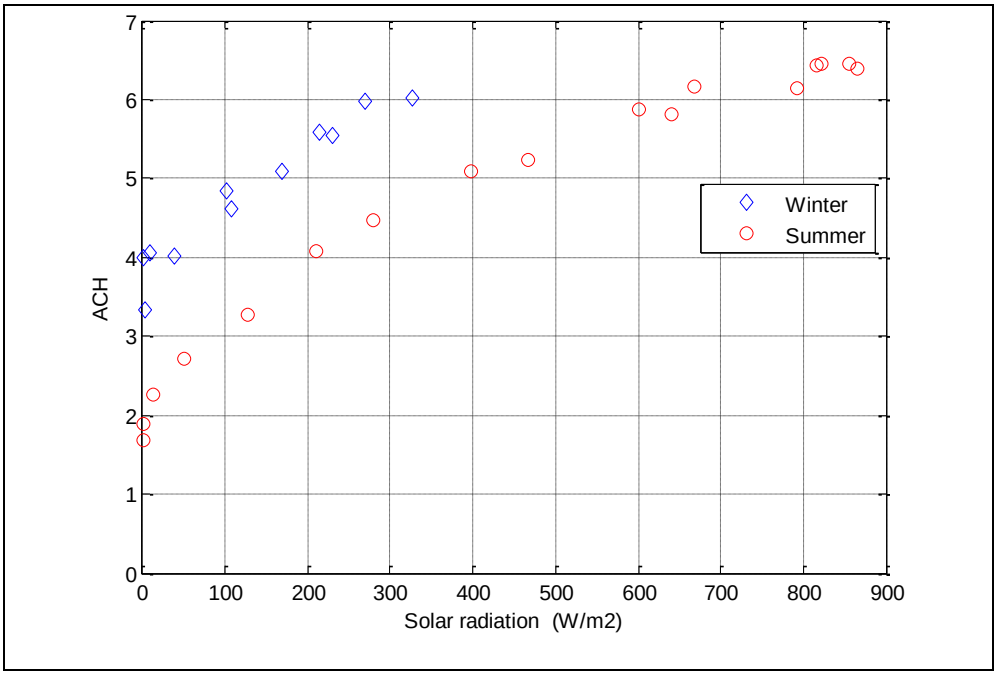

Figure 13. Effect of solar radiation in attic ventilation rate (for cases with stack effect)

6.3.1 Effect of Insulation Thickness on Attic Ventilation

To investigate the effect of insulation thickness on attic ventilation rates, two additional simulation cases with R45 (RSI-7.9) and R60 (RSI-10.6) were carried out. Figure 14 shows the mass flow rates and the ACH at different hours in the attic roof with R30, R45, and R60. The figure on the left (Figure 14) shows that as insulation thickness increases, the airflow rate through the attic space tends to decrease slightly. This must be attributed to the reduction of heat flow from the conditioned space to the attic space, which results in low insulation surface and attic air temperatures. Although the flow rate slightly decreases with insulation thickness, as can be seen in the figure on the right (Figure 14), the ACH is slightly higher in the attic with higher insulation values when solar radiation gain is higher. The main reason for the slight increase of ACH is due to the reduction of the attic space volume due to the addition of extra insulation thickness. In general, however, the attic ventilation rates in the three simulation cases are not significantly different.

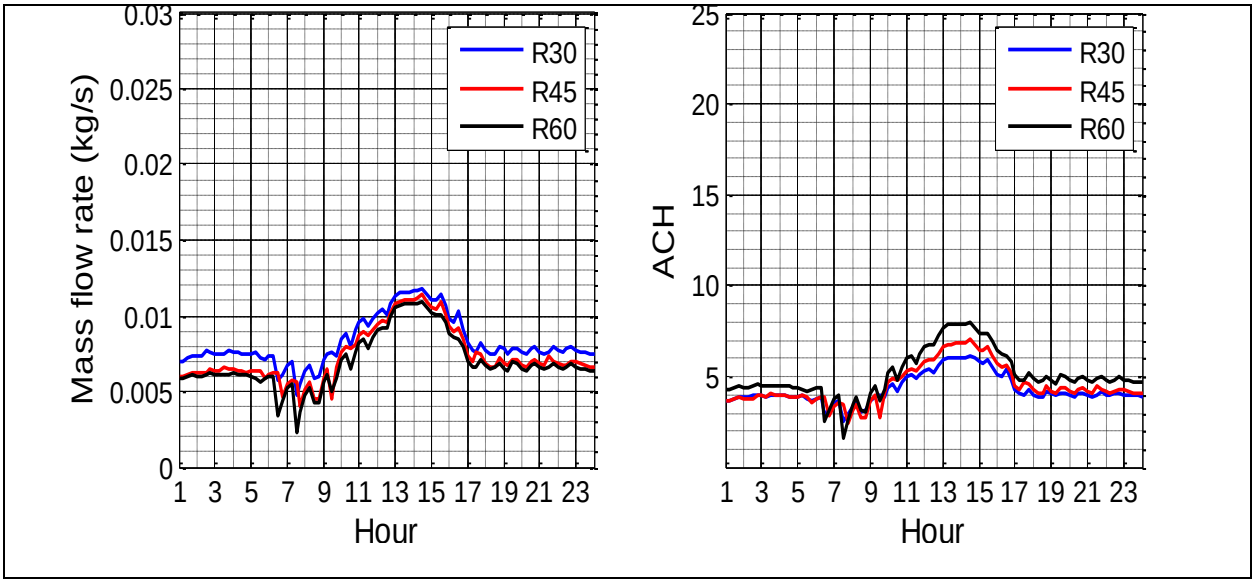

Figure 14. Attic ventilation rates with different insulation thickness

6.3.2 Effects of Baffle Size in Attic Ventilation

Most building codes recommend a minimum 1-inch gap between the roof sheathing and the insulation. To investigate the effect of baffle size (air gap) on attic ventilation, three simulation cases with 1" (25 mm), 2" (50 mm), and 3" (75 mm) baffles were considered. The simulation results suggest that varying the baffle size influences the attic air distribution but has a lesser effect

on attic air temperature. Figure 15 shows the air distribution in three attics with different baffle sizes during a summer condition with a wind speed of 2 m/s entering through the left soffit vent. As shown in the figure, the air velocity in the attic increases as the baffle size increases. The flow patterns in the corresponding attics are also quite different. The ACH values for the three baffle sizes are shown in Figure 16. From the graph, it can be deduced that the gap between the underside roof sheathing and insulation has a significant influence on attic air change rates when the ventilation is driven by wind. The ACH value increases as the baffle size increases. The ACH in the attic with 2" and 3" baffles is found to be 38.5% and 52.5%, respectively, higher than that of an attic with a 1" baffle. However, similar simulation results suggest that the effect of baffle size is not significant when the ventilation is driven by a stack-effect. In the buoyancy-driven ventilation scenario, the airflow is caused by the difference of the top of insulation and roof sheathing temperatures. This means the change in baffle size does not considerably affect the airflow distribution and ACH.

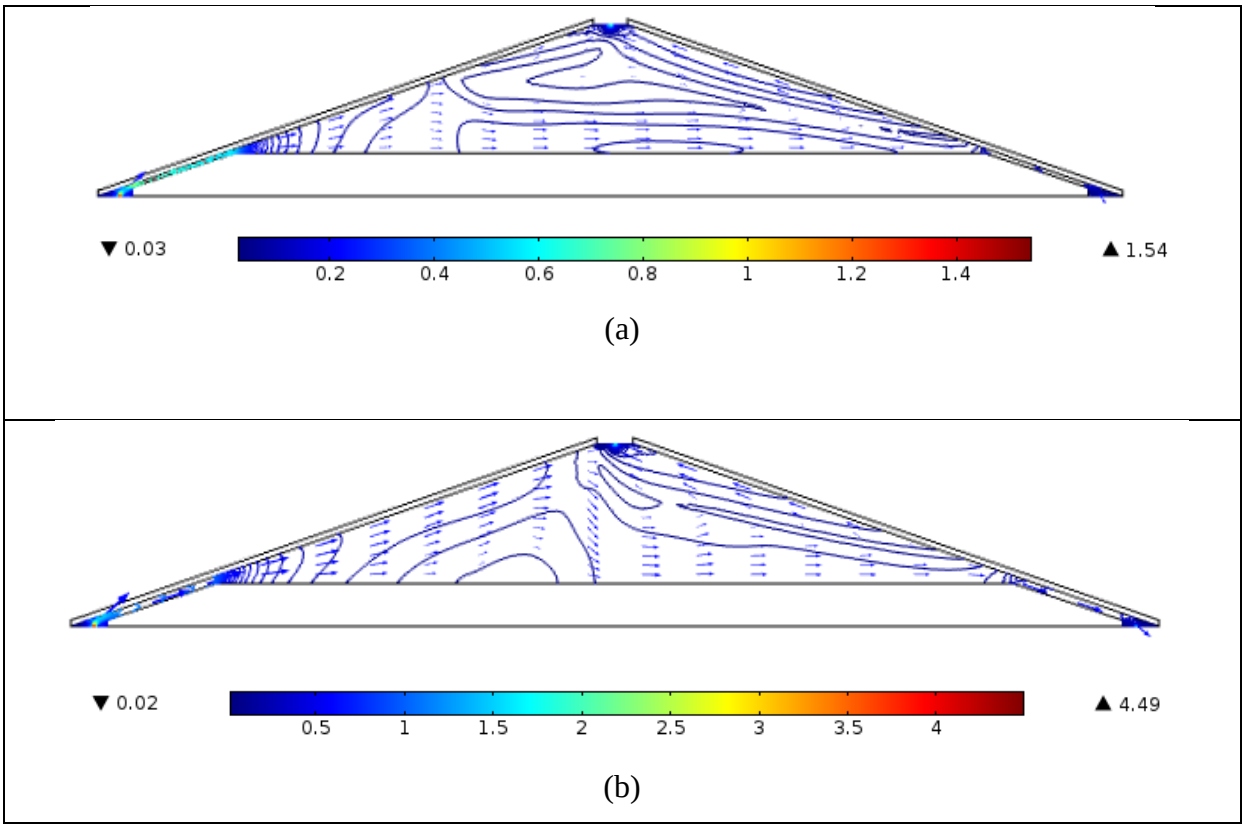

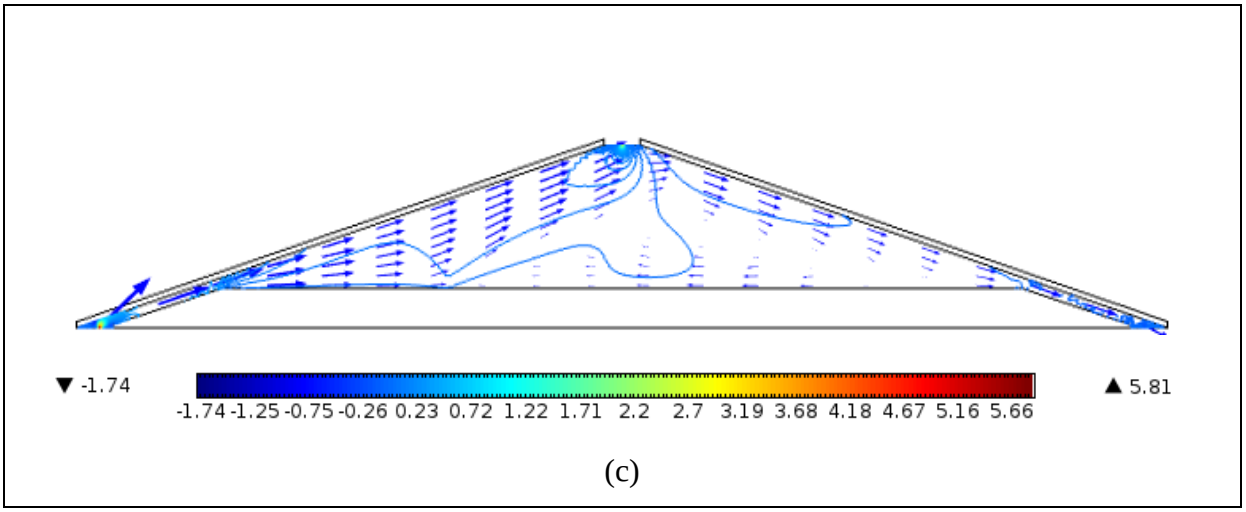

Figure 15. (a) - (c) air distribution in wind driven attic ventilation with an attic of baffle size 1 in, 2 in and 3 in respectively

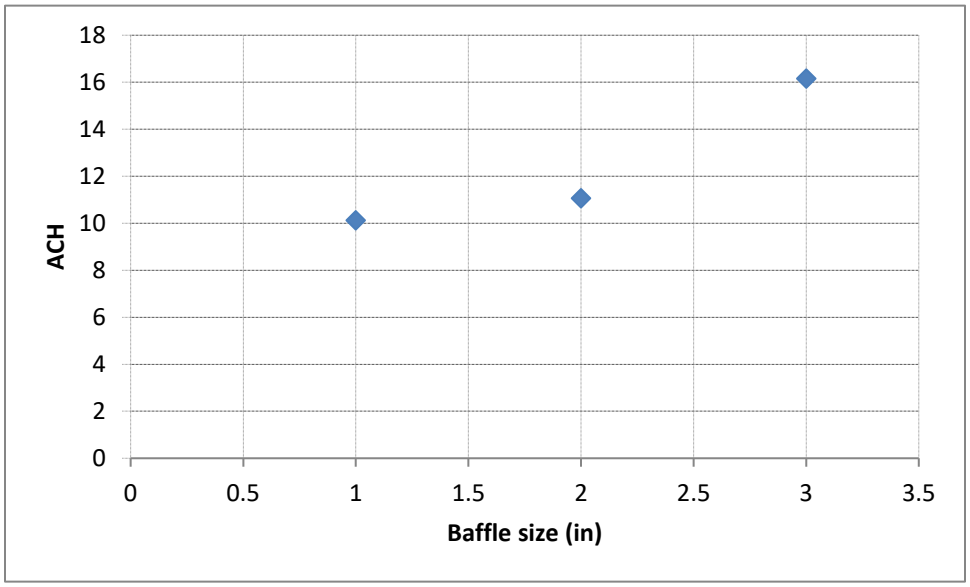

Figure 16. Attic ventilation (ACH) vs attic baffle sizes with 2.0 m/s wind

6.4 Heat Flow through Attic Floor

Figure 17 shows the heat fluxes along the attic floor-length at 12:00 am for the sealed attic, buoyancy-induced, and wind-induced attic ventilation scenarios. The sharp increase in heat flux close to the ends is due to the two-dimensional heat flow and the reduced insulation thickness at the edges. The heat flux profiles away from the edge seem to correlate with the airflow patterns shown at the same time, Figure 8 (page 26). Although not that significant, the locations where two airflow patterns meet in the sealed and buoyancy-driven attic ventilation cases (Figure 8, a and b) are the same locations where slight changes in the heat flux profiles are observed in Figure 17. Similarly, the points where the cold air jet touches down on the insulation in the cases of wind-induced attic ventilation scenarios (Figure 8, c and d), are the same points where the heat fluxes show an increase in the corresponding cases.

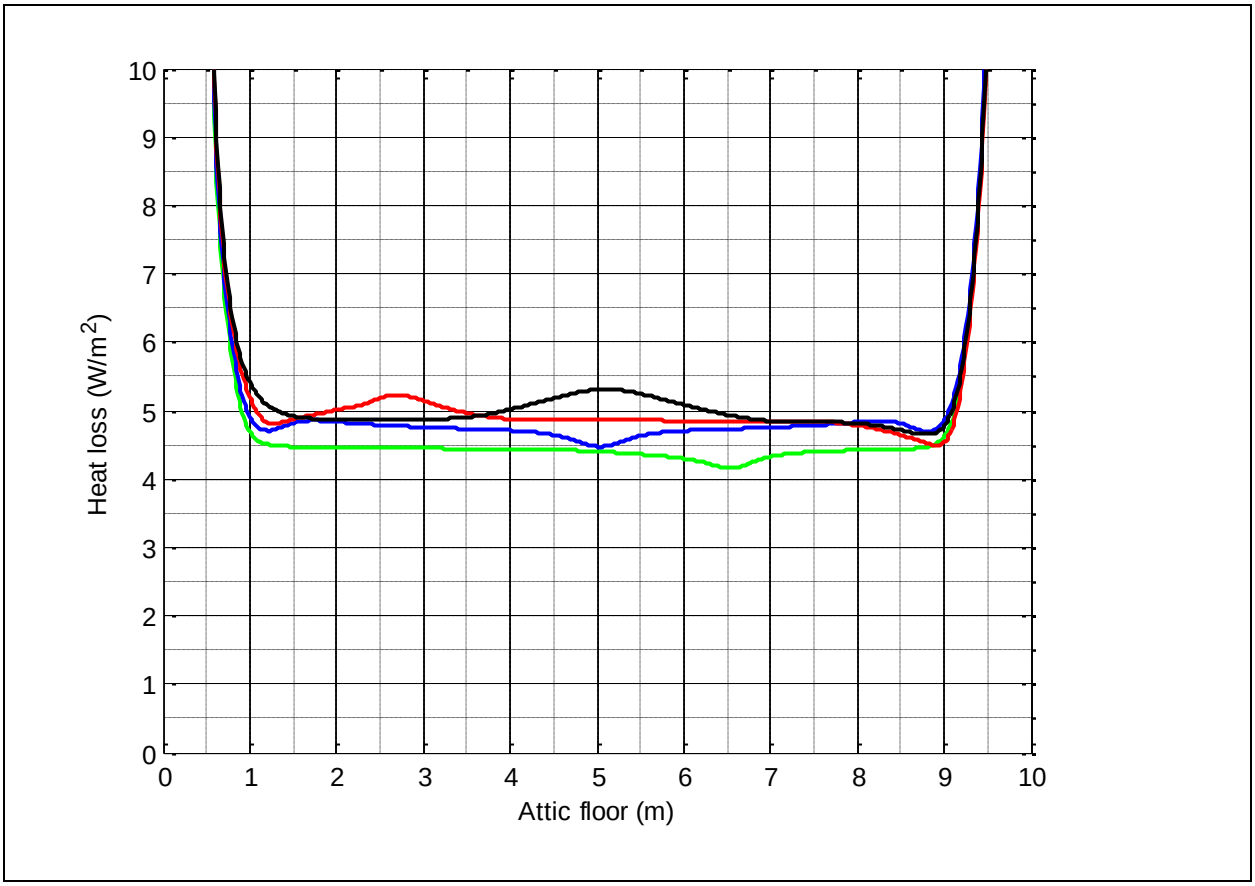

Figure 17. Heat flux along the attic floor at 12:00 am (winter day--Ottawa). Color code: green (sealed), blue (stack effect), red (0.6Pa wind pressure), black (2Pa wind pressure)

The hourly heat loss and gain through the attic roof during the winter and summer days are presented in Figure 18. As can be seen in both figures, heat flow through the sealed attic is higher than in both buoyancy- and wind-ventilated attic roofs. The heat flux differences among the four scenarios reach the highest at 4:00 pm. This time corresponds to the lowest and the highest heating and cooling demands in the winter and summer days, respectively. The thermal energy storage capacity of the sealed attic is beneficial in the winter while it is disadvantageous in the summer period as it increases cooling load. Based on the boundary conditions used in this report, the daily total heat loss through the attic floor in winter in cases with buoyancy-driven, 0.6 Pa, and 2 Pa wind pressure conditions are 6.8%, 9.6%, and 11.6%, respectively—higher than that of the sealed attic. In the summer, the cooling loads in the corresponding vented attic operation conditions are lower by 39%, 40%, and 46%, respectively, when compared to the sealed attic. As can be seen in the figures, higher attic ventilation rates due to wind pressure 10 ACH (0.6 Pa pressure) and 20 ACH (2 Pa wind pressure) do not significantly change the heating and cooling demands. In fact, from the energy-saving (both heating and cooling) perspective, an attic roof with only buoyancy-driven ventilation (sheltered from the wind) may perform better. Of course, for attic moisture control, higher attic ventilation rates may be preferred.

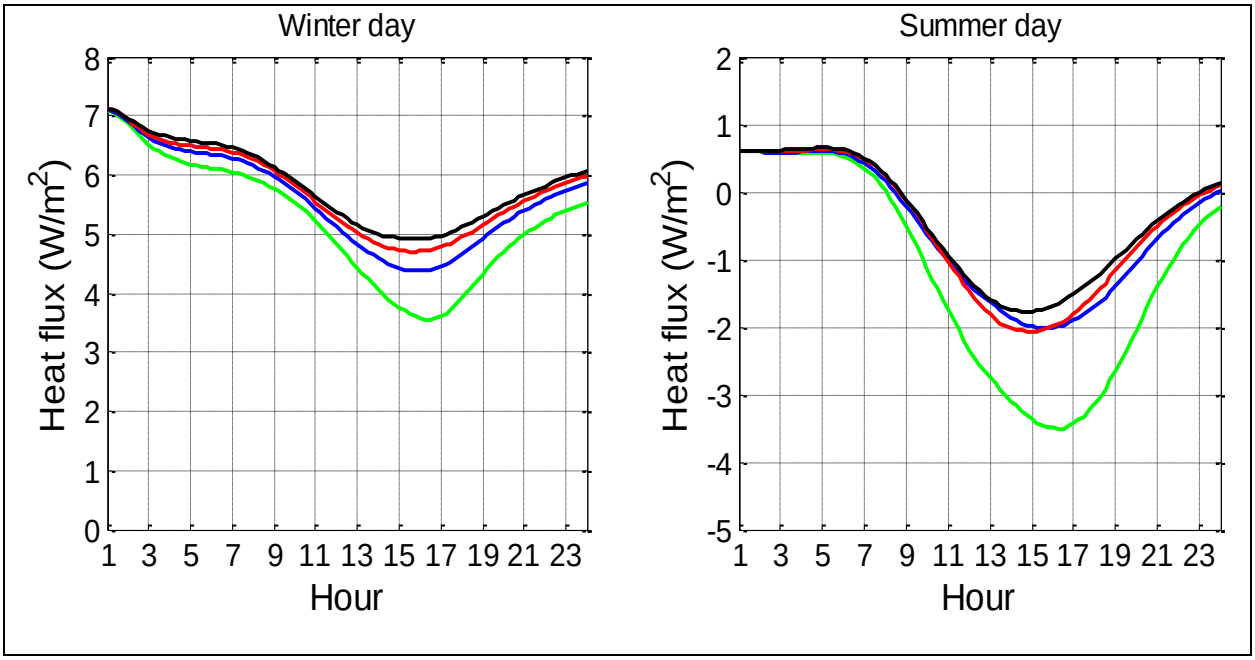

Figure 18. Hourly heat flux through attic floor for different attic ventilation scenarios during a typical winter and summer day (Ottawa). Color code: green (sealed), blue (stack effect), red (0.6Pa wind pressure), black (2Pa wind pressure)

6.5 Moisture in Attic Roof

In this section, the combined heat-air-moisture transfer in the attic roof is studied, and the hygrothermal responses of a moisture-sensitive component, roof sheathing, is presented. For the study, the same roof system described in Section 4 is considered. As Figure 8 and Figure 9 show, the temperature and flow patterns in the attic are not uniform. Accordingly, the heat, air, and moisture distributions in the attic roof are mapped by employing conjugate heat-air-moisture (HAM) transfer analysis. The approach involves the coupling of the CFD model discussed in Section 2 and the benchmarked HAM model HAMFit [5] for the attic air space and roof deck, respectively. The mathematic models implemented in HAMFit are given below for completeness.

6.5.1 Mathematical Model (Heat-Air-Moisture Transport Model)

The HAMFit model solves, simultaneously, the three interdependent transport phenomena of heat, air, and moisture in a building component. The mathematical model is based on building physics and comprises a set of partial differential equations (PDEs) that govern the individual flows, which are presented below:

Moisture balance:

$$\theta \frac{\partial \emptyset}{\partial t} = \nabla.(D_{\emptyset} \nabla \emptyset + D_t \nabla \mathrm{T}) - \nabla.(\mathrm{D}_t \rho_w \vec{g} + \rho_a \vec{u} C_c \hat{P} \emptyset) \quad (1)$$

where $D_{\emptyset} = \left(+D_t \frac{\rho_w RT}{M\emptyset}\right)$, $D_r = \left(\delta_r \frac{\widehat{\partial P}}{\partial T} + D_t \frac{\rho_w R}{M} \ln(\emptyset)\right)$ and $C_c = \frac{0.622}{P_{atm}}$

Heat balance:

$$\rho_w C_{Peff} \frac{\partial T}{\partial t} + \nabla.(\vec{u}T)\rho_a\left(C_{pa} + \omega C_{pr}\right) + \nabla.\left(\lambda_{eff} \nabla T\right) = \dot{m}_c h_{fg} + \dot{m}_c (Cp_v - Cp_l) + \dot{Q}_s \quad (2)$$

where $C_{Peff} = Cv_m + y_l C_{Pl}$ and $\dot{m}_c = \nabla.(\delta_v \nabla P_v) - \rho_a \nabla.(\vec{u}\omega)$

Air mass balance:

$$\nabla.(\rho_a \vec{u}) = 0 \quad (3)$$

Momentum balance (Darcy equation):

$$\vec{u} = \frac{k_a}{\eta} \nabla P \tag{4}$$

$$-\nabla . \left(\rho_a \frac{k_a}{\eta} \nabla P \right) = 0 \tag{5}$$

where: ρ_w : density of water (kg/m^3), ρ_a : density of air (kg/m^3), θ : sorption capacity (kg/m^3), $\emptyset$: relative humidity, $\vec{u}$: air velocity (m/s), h_{fg} : latent heat of evaporation/condensation (J/kg), $\hat{P}$: saturated vapour pressure (Pa), δ_v: vapour permeability (s), ω: humidity ratio (kg/kg air), k_a: air permeability (m^2), η: dynamic viscosity (kg/ms).

The governing partial differential equations (PDEs) of the three transport phenomena (Equation 1, Equation 2, and Equation 5) are coupled and solved simultaneously for temperature, relative humidity, and pressure using COMSOL, a finite-element-based software.

6.5.2 Simulation Setup

The hygrothermal responses of the attic roof sheathing are studied for cases in which ceilings are either with or without air leakage and attic roofs with different cellulose insulation thickness (R30, R50, and R60) shown in Figure 19. These R-values are selected to represent a house built before the current building code, a building built to the current code, and a highly insulated roof building, respectively. For the study, a case in which the plywood sheathing will be at more risk of moisture damage due to air leakage is considered, which is a scenario when attic ventilation is low. As presented previously, buoyancy-driven attic ventilation is much lower than wind-induced ventilation. Accordingly, in this study, the coupled CFD-HAM simulations are run for a buoyancy-induced flow case. In this case, as can be seen in Figure 20, warm air rises at the middle of the roof, touches the ridge, and flows back down along the sheathings' surfaces. This airflow pattern suggests that air leakage at the center of the ceiling may result in more moisture damage (condensation) on the sheathing than other locations. This is because air leakage at other locations needs to travel a longer distance before coming in contact with the sheathing, and along its long path it will lose its moisture concentration by diffusion to the attic space air. Accordingly, in this study, air leakage at the center of the attic roof is considered. Based on the data presented in Sheltair (1997) [11], a Normalized Leakage Area (NLA) of 2.4 cm^2/m^2 is used for the study.

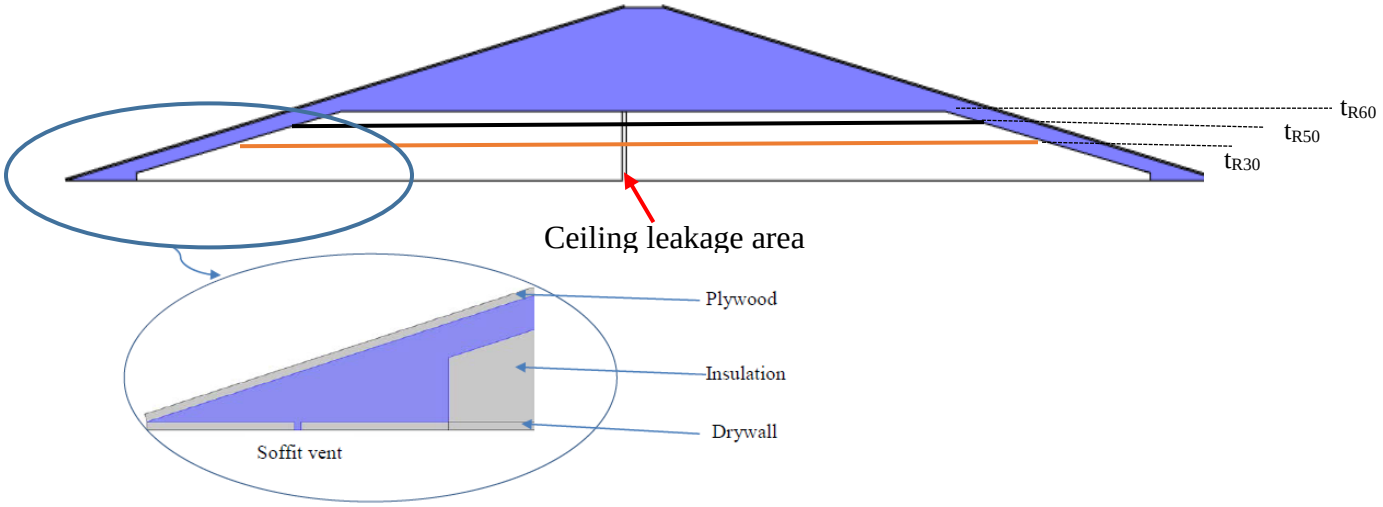

Figure 19. Geometrical model of the attic. t_{R30}, t_{R50}, t_{R60} are thicknesses of R30, R50, and R60 insulations, respectively.

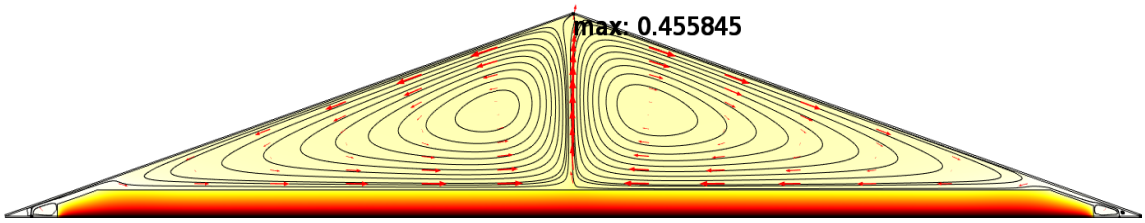

Figure 20. Airflow pattern in an attic space: a case with no external driving forces (only solar and wind)

In consideration of the high computational demand and the long convergence time required for a coupled and transient CFD-HAM modeling on the one hand and the slowness of the moisture transfer process (higher time constant in comparison to air or heat flow) on the other hand, the simulation period is set for one winter week. To assess the attic performance in a cold climate, a location in Climate Zone 7A, Prince George, Northern BC, is selected for the analysis. The outdoor temperature and the relative humidity data of Prince George used in the study are shown in

Figure 21. In addition to these boundary conditions, the longwave radiation exchange between the roof surface and the sky and solar radiation on the surfaces is considered in the simulation.

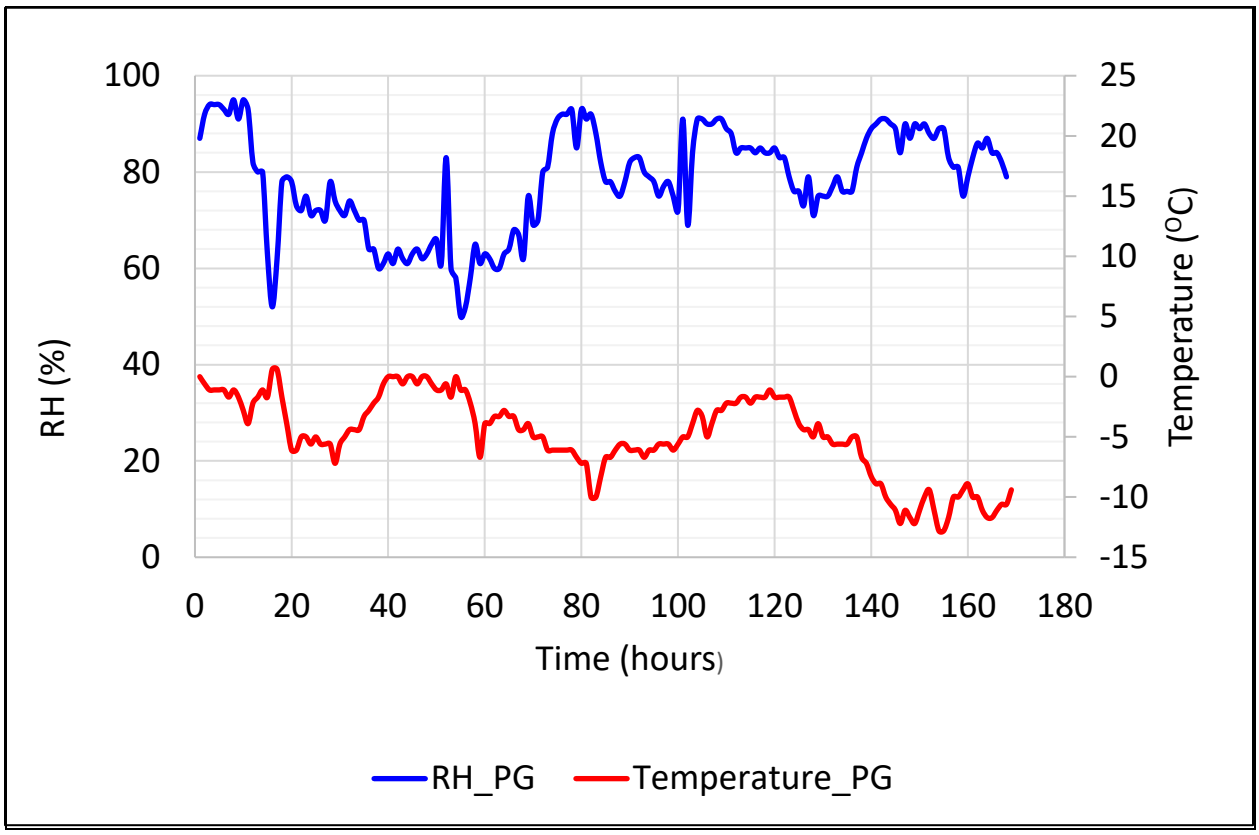

Figure 21. The outdoor temperature and relative humidity used for the study.

The hourly indoor temperature and RH values for the occupied space below are determined for normal occupancy density using the ASHRAE 160 Intermediate model (Equation 9).

$$p_i = p_{o,24h} + \frac{c\dot{m}}{Q} \tag{9}$$

where p_i = indoor vapor pressure, $p_{o,24h}$ = 24-hour running average outdoor vapor pressure, c = 1.36 × 105 Pa·m3/kg, $\dot{m}$= design moisture generation rate, Q = design ventilation rate. The indoor air temperature is set at 21^{O}C, and 0.1 ACH is used to calculate the design ventilation rate.

6.5.3 Simulation Results

The following section presents the hygrothermal performance of a roof sheathing with and without air leakage and three different insulation thicknesses for climate Zone 7A – Prince George.

The effects of the air leakage on roof sheathing moisture accumulation are studied using the relative humidity values on the north-facing roof. The reason behind selecting the north-facing roof is to examine the performance of a roof sheathing under minimal solar radiation or low drying potential conditions. Figure 22 shows the relative humidity distribution on the roof sheathing for different insulation thicknesses after the 7th day of the start of the simulation.

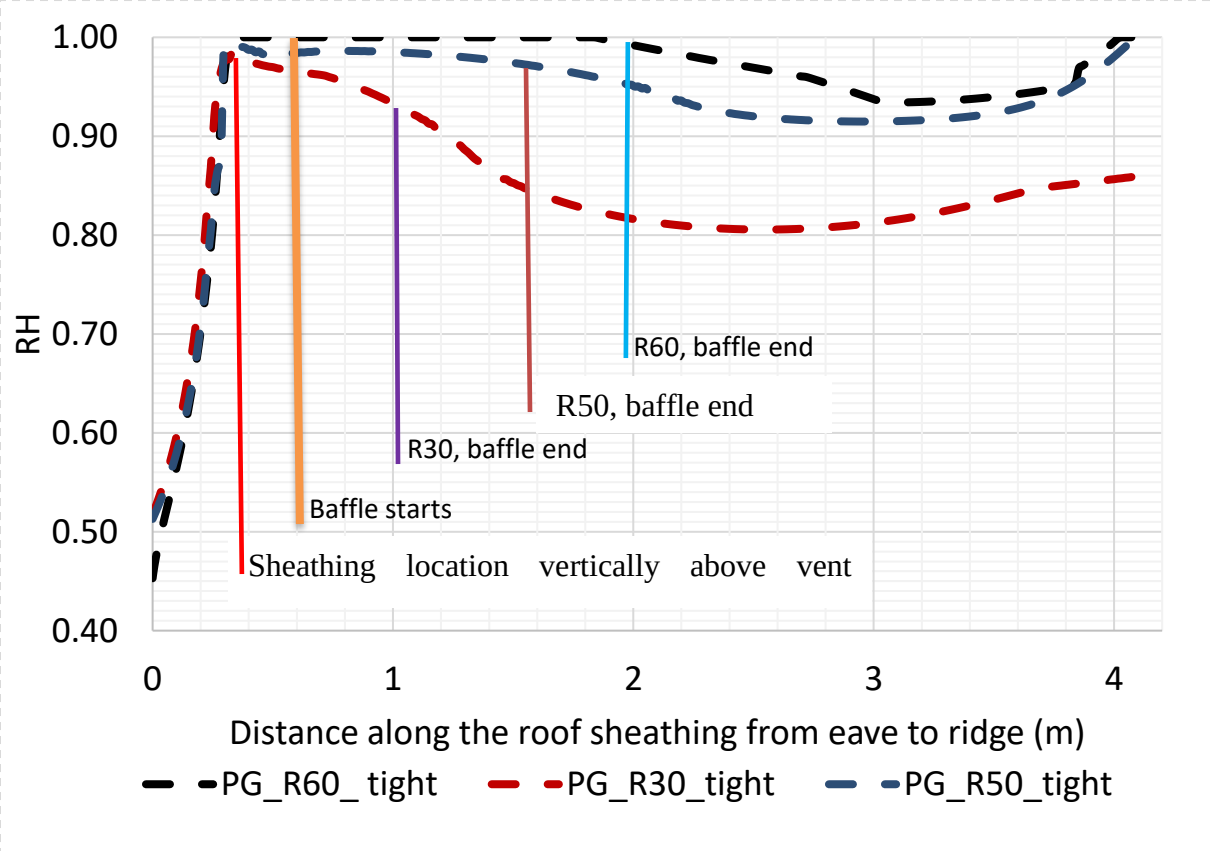

Figure 22. RH values of a roof sheathing under different insulation, Prince George

As can be seen in the figure, the sheathing's relative humidity in the attic with R60 insulation reaches 100% near the baffle region and near the ridge. The attics with R50 and R60 insulation attain more than 90% of relative humidity in most zones of roof sheathing. This is due to the combined effect of night-time cooling from longwave radiation exchange of the sheathing with the cold sky and the low heat flow from the occupied space to the sheathing due to the high attic

insulation level. The relative humidity of the sheathing board on the R30 attic decreases rapidly beyond the baffle. A maximum RH difference of 18% and 5% is registered by R30 and R50 attics, respectively, in comparison to the attic with R60 insulation. Although the magnitude of moisture accumulations on the sheathing vary, the moisture distribution profiles in all three insulation cases are similar: higher at the baffle and near ridge locations and lower at the middle section of the sheathing. This moisture profile is consistent with the airflow pattern observed in Figure 20. The locations on the sheathing where the air starts to flow upward or reverse its direction and flow downward (at baffle and near ridge locations, respectively), the air transfers most of its moisture to the sheathing. The RH value remains similar for all the three attic insulation thicknesses in the region between the eave and the sheathing place directly above the soffit vent.

In order to assess the effect of ceiling air leakage on the hygrothermal performance of the roof sheathing, three distinct locations on the sheathing board are selected, and their RH and mould index evolution with time. Figure 23 shows the relative humidity values of the roof sheathing at the three locations for cases with and without ceiling air leakage. The selected locations are vertically above the center of the baffle (location ‘A’); midway through the board (location ‘B’); and near the ridge (location ‘C’). As shown in the figure, the plywood at location ‘A’ attained a 100% RH value starting from the 119^{th} and 153^{rd} hours for the airtight and leaky attics, respectively. While similar relative humidity values are observed at location ‘B’ and ‘C’ in the airtight ceiling case, up to a 5% relative humidity difference between the two locations is observed in the leaking ceiling case. In general, the effect of air leakage is more pronounced at location ’C’ near the ridge than the middle or baffle locations. At this location, a difference of about 8% relative humidity is observed between the leaky and the tight ceiling cases. In all three locations, the relative humidity reaches a higher value in leaky attics more quickly than in tight ceilings.

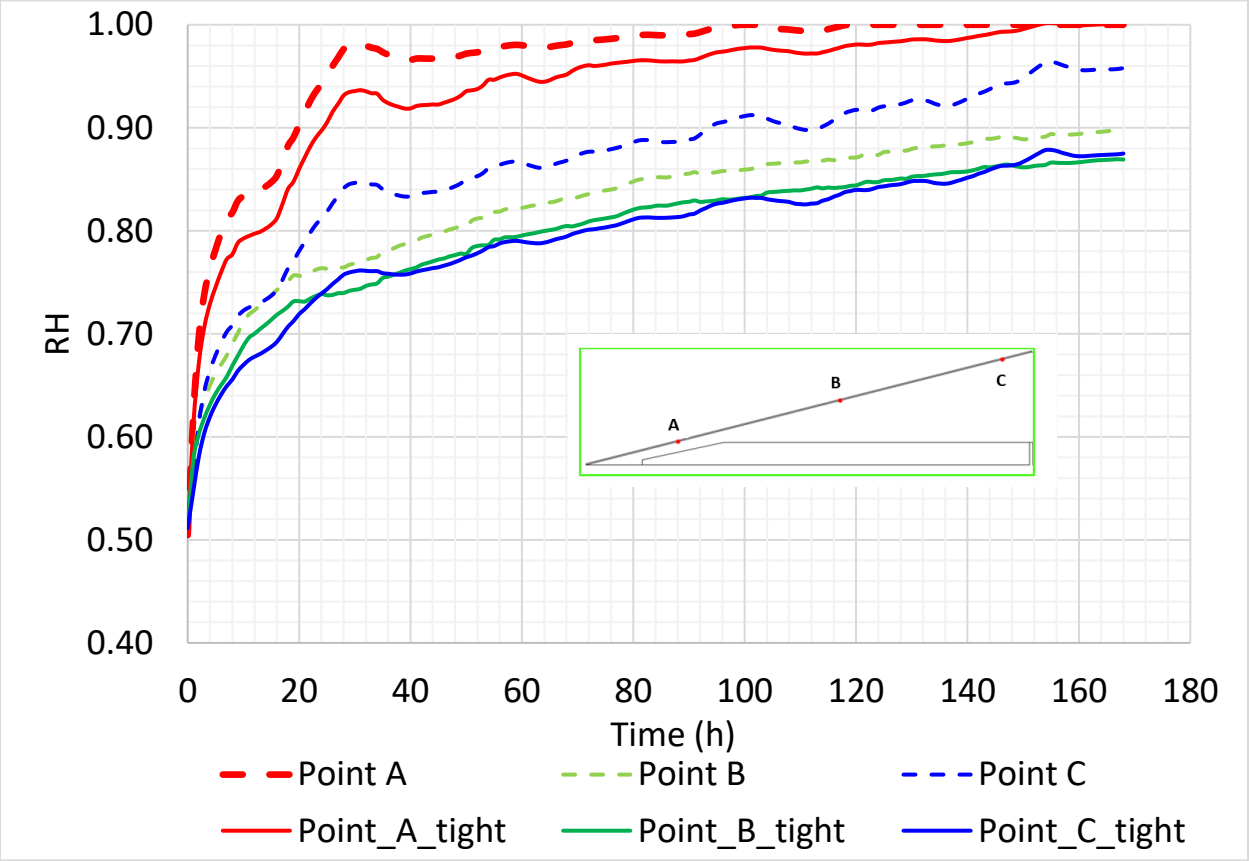

Figure 23. RH values of roof sheathing at different locations

7. Conclusion

In this report, the behavior of air and temperature distribution inside the attic and moisture on the attic sheathing are examined. A two-dimensional CFD model using COMSOL is developed and benchmarked against existing experimental data. The air exchange per hour (ACH) in attic space under four different attic ventilation scenarios are computed. In the absence of wind and solar radiation, buoyancy-induced ventilation in the winter is more than two times that of the summer. In the absence of wind, attic ventilation increases as solar radiation increases. For scenarios with wind pressure of 0.6 Pa and 2 Pa, the attic ventilation rate in the winter increases by 2.5 and 5.0 times the ventilation in the scenario with no wind pressure (only stack effect). Unlike buoyancy-induced ventilation, wind-induced ventilation is less sensitive to solar radiation. In general, baffle size (size of air gap between the roof sheathing and insulation) has an impact on attic ventilation rate and airflow distribution but has a lesser effect on attic air temperature. The effect of baffle

size is not significant when the ventilation is driven by a stack-effect. The airflow path and temperature field in attic space are significantly affected by solar radiation. In the absence of solar radiation, relatively high wind pressure (2 Pa in this report) forces the incoming air to flow underneath of the sheathing and exit at the ridge vent, which consequently reduces the time of residence of the incoming air and its subsequent mixing with the air in the attic space. The simulation results also show that attic ventilation in winter poses an energy penalty, whereas in the summer, it helps to remove the hot air from the attic space and reduce cooling load and energy demand.

The results of the combined two-dimensional CFD and hygrothermal modeling suggest that a highly insulated attic increases the moisture content in the roof sheathing. With R30 insulation, the relative humidity on the roof sheathing was below 90% except near the attic baffle. In all three attic insulation cases (R30, R50, and R60), the relative humidity value spikes near the ridge vent. Air leakage at the center of a ceiling has a more pronounced effect in the upper section of the roof sheathing, and its effect in the lower part of the sheathing is negligible. Areas near the attic baffle are the most vulnerable regions for moisture-related problems. Accordingly, more focused studies should be undertaken to generate technical solutions to address the moisture problems around the baffle and near the ridge.

8. References

[1] Roodvoets, D. L. (2001). *Practical implications of the elimination of natural attic ventilation in mixed climates*. Performance of Exterior Envelopes of Whole Buildings VIII Conference Proceedings (ASHRAE), Florida, United States.

[2] Forest, T. W., & Walker, I. S. (1993). *Attic ventilation and moisture*, Final Report submitted to Canada Mortgage and Housing Corporation, Ottawa, Canada.

[3] Lstiburek, J. (2014). *Understanding attic ventilation*. http://www.buildingscience.com/documents/digests/bsd-102-understanding-attic-ventilation.

[4] Tariku, F., Kumaran, M. K., & Fazio, P. (2010). Transient model for coupled heat, air and moisture transfer through multilayered porous media. *International Journal of Heat and Mass Transfer, 53*(15–16), 3035-3044.

[5] Chen, Q. (1996). Prediction of Room Air Motion by Reynolds-Stress Models, *Building and Environment*, 31, 233-244.

[6] Flack, R. D., & Witt, C. L. (1979). Velocity measurements in two natural convection air flows using a laser velocimetery. *ASME J. Heat Transf, 101*, 256–260.

[7] Flack, R. D. (1980). The experimental measurement of natural convection heat transfer in triangular enclosures heated or cooled from below. *ASME J. Heat Transf, 102*, 770–772.

[8] National Research Council Canada (NRC-IRC). (2015). *National building code of Canada (NBC)*. Ottawa, ON, Canada. https://nrc.canada.ca/en/certifications-evaluations-standards/codes-canada/codes-canada-publications/national-building-code-canada-2015.

[9] National Research Council Canada (NRC-IRC). (1997). *Model national energy code of Canada for houses (MNECC).* Ottawa, ON, Canada. https://shop-magasin.nrc-cnrc.gc.ca/

[10] ASHRAE. (2013). *ASHRAE Handbook—Fundamentals.* Atlanta, United States.

[11] Sheltair Scientific Ltd. (1997). *Attic ventilation and moisture control strategies*. Final Report, Canada Mortgage and Housing Corporation (CMHC), Ottawa, Canada.

9. Appendix A: Simulation results for mild climate conditions

Attic temperature

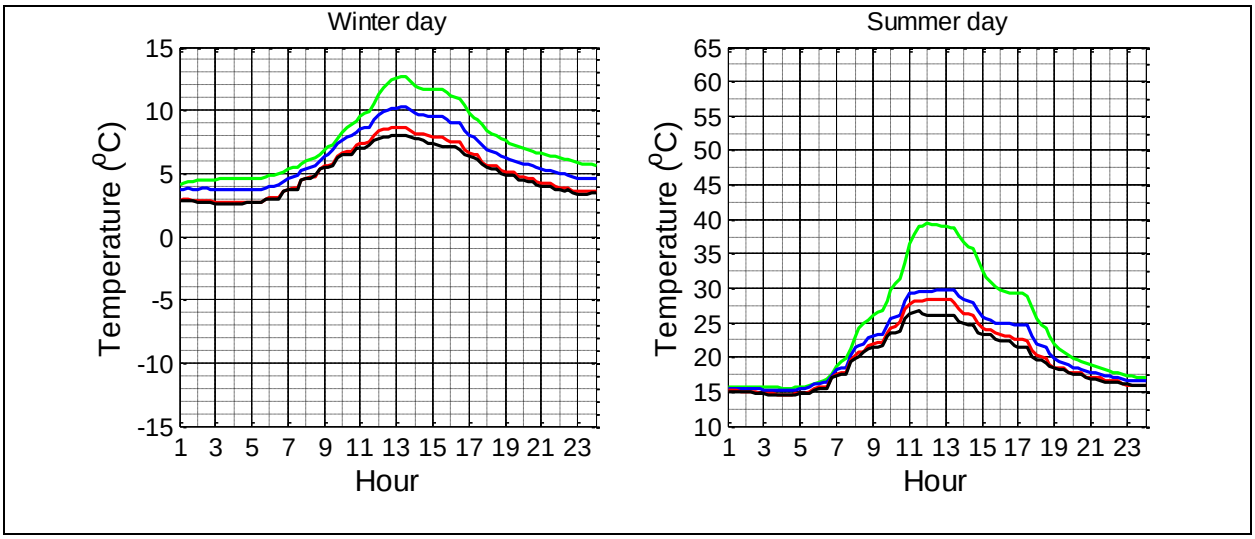

Figure 24 Average attic air temperature for different attic ventilation scenarios during a typical winter and summer day—Mild climate (Vancouver). Color code: green (sealed), blue (stack effect), red (0.6 Pa wind pressure), black (2 Pa wind pressure)

Roof sheathing temperature

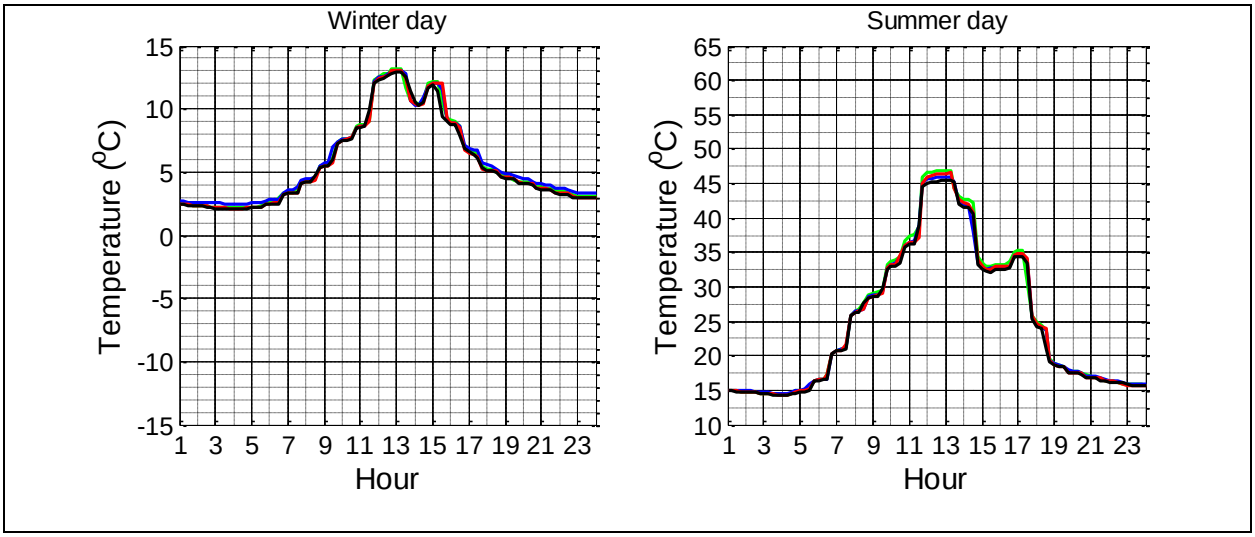

Figure 25. Maximum roof sheathing temperature for different attic ventilation scenarios during a typical winter and summer day—Mild climate (Vancouver). Color code: green (sealed), blue (stack effect), red (0.6 Pa wind pressure), black (2 Pa wind pressure)

Attic ventilation rate

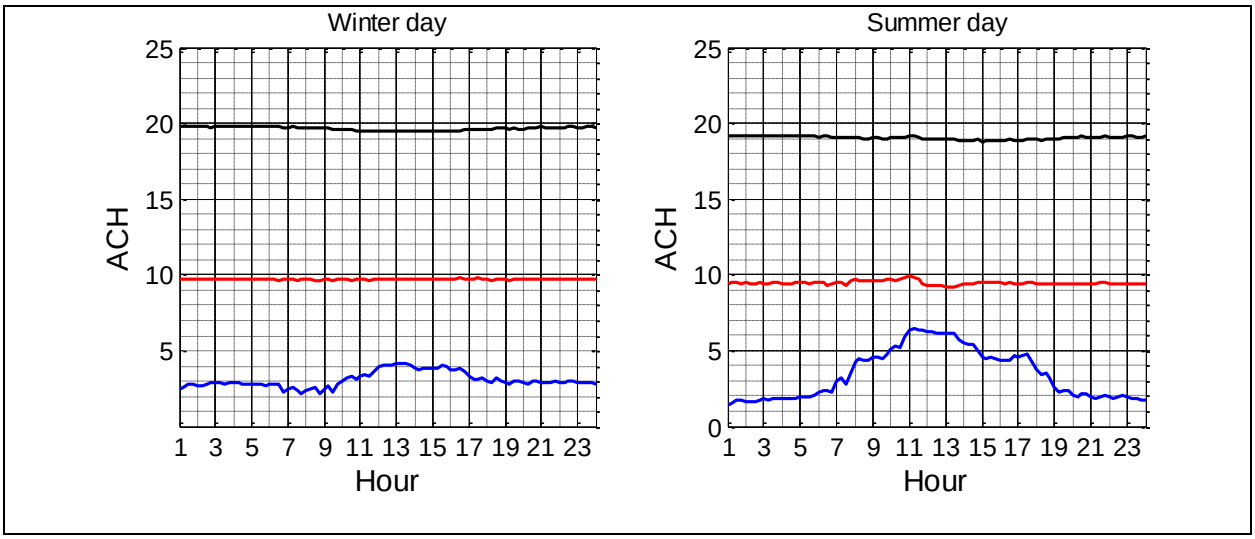

Figure 26 Attic ventilation rates for different attic ventilation scenarios during a typical winter and summer day—Mild climate (Vancouver). Color code: blue (stack effect), red (0.6 Pa wind pressure), black (2 Pa wind pressure)

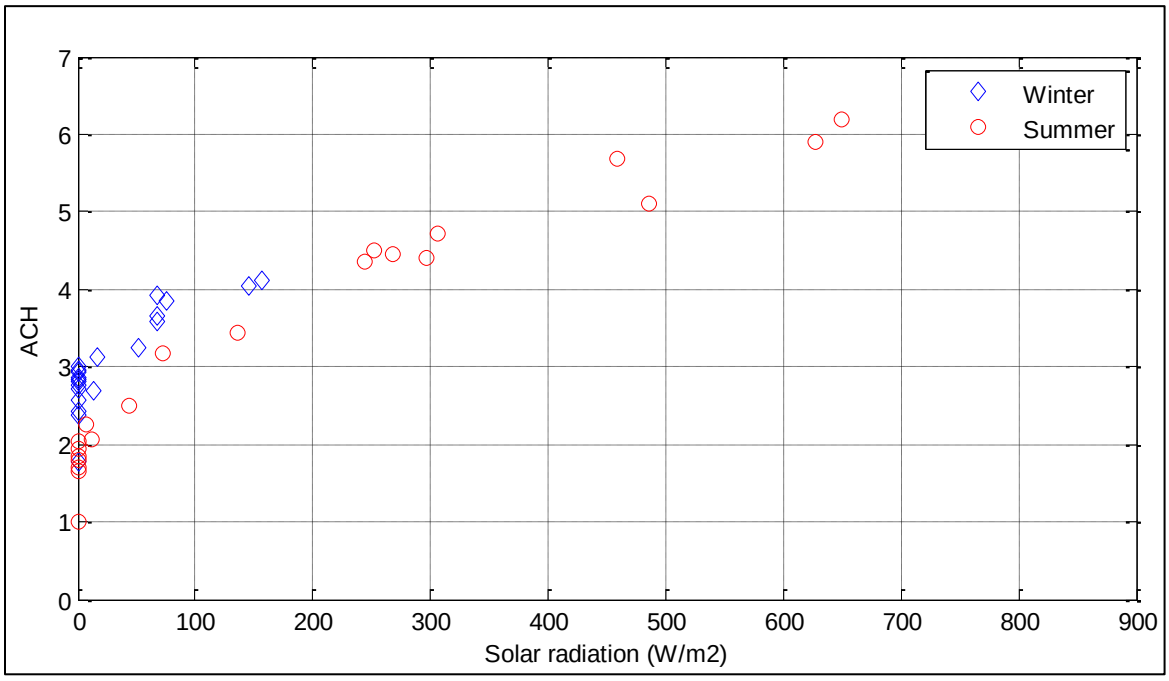

Figure 27 Effect of solar radiation in attic ventilation rate (for cases with stack effect)—Mild climate

Heat flow through attic floor

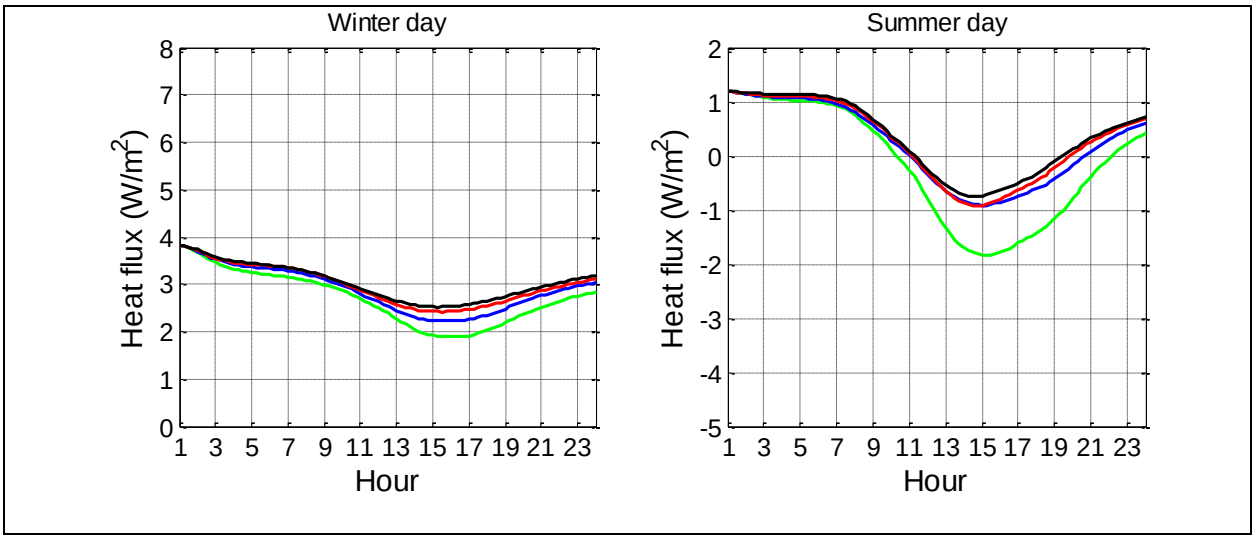

Figure 28 Hourly heat flux through attic floor for different attic ventilation scenarios during a typical winter and summer day—Mild climate (Vancouver). Color code: green (sealed), blue (stack effect), red (0.6 Pa wind pressure), black (2 Pa wind pressure)